communications earth & environment

Article

A Nature Portfolio journal

https://doi.org/10.1038/s43247-025-02667-6

Biomarker evidence of a serpentinite chemosynthetic biosphere at the Mariana forearc

Palash Kumawat [1] ✉, Elmar Albers [2,6], Wolfgang Bach [1,3], Frieder Klein [4], Walter Menapace [5,7], Christoph Vogt [1,3] & Florence Schubotz [3]

Present-day serpentinization systems, such as that at the Mariana forearc, are prominent sources of reduced volatiles, including molecular hydrogen (H_2) and methane (CH_4), and are considered analogs for chemosynthetic ecosystems on early Earth. However, seepage of serpentinization fluids through mud volcanoes at the Mariana forearc seafloor is defined by high pH, and nutrient scarcity, creating challenging conditions for microbial life. We present geochemical and lipid biomarker evidence for a subsurface biosphere shaped by episodic substrate availability, highlighting microbial persistence across steep geochemical gradients within serpentinite mud. Light stable carbon isotope compositions from diagnostic lipids reveal a temporal shift from hydrogenotrophic methanogenesis to sulfate-dependent anaerobic methane oxidation. Membrane adaptations, including unsaturated diether, acyclic and branched tetraether, and ether-based isoprenoidal and non-isoprenoidal glycosidic lipids, reflect microbial strategies for coping with this extreme environment. Our findings establish the Mariana forearc as a unique serpentinite-hosted biosphere, where life operates at the fringes of habitability.

The subseafloor biosphere is estimated to harbor up to 15% of the global biomass[1]. Recent advances in deep biosphere research have improved our understanding of the distribution and diversity of microbial life in the rocky oceanic crust, especially around hydrothermal vents[2,3]. This subseafloor biosphere has to adapt to limited carbon and nutrient availability, accompanied by harsh environmental conditions such as high temperature and pressure, elevated salinity, and/or extreme pH levels[4]. Serpentinization of mantle rocks by seawater can generate high levels of H_2[5,6] that, in turn, drives the abiotic reduction of carbon to form CH_4 and other organic compounds[7], which can be oxidized by chemosynthetic organisms[8–10], forming the foundation for a serpentinite biosphere[11]. The type locality for such a serpentinite biosphere is the Lost City hydrothermal vent field near the Mid-Atlantic Ridge, where hydrothermal fluids fuel microbial communities in active and inactive vent structures[12]. Methanogenic archaea there are found in active brucite-calcite vents, whereas older carbonate chimneys host a syntropic consortium of anaerobic methanotrophic archaea (ANME) and sulfate-reducing bacteria (SRB) that perform the anaerobic oxidation of methane (AOM)[13,14].

The process of serpentinization takes place in a range of geotectonic settings, including rifted continental margins, mid-oceanic ridges, transform faults, and convergent margins. Among the latter, the forearc of the Mariana subduction system is of particular interest because it provides access to serpentinization products from within an active subduction zone. There, dewatering of the subducting Pacific Plate leads to serpentinization of the mantle wedge of the overriding Philippine Sea Plate. Faults reaching 10–25 km deep into the forearc allow serpentinite, together with fluids derived from the subducting slab, to buoyantly rise and form large 'serpentinite mud volcanoes' on the seafloor[15,16] (Fig. 1a, c). Fluids venting from the mud volcanoes are cold (<3.5 °C), hyperalkaline (pH up to 12.6), and enriched in H_2 and CH_4 (both up to ~1 mM)[17,18] and slab-derived sulfate (SO_4^{2-}; up to 28 mM)[19]. These fluids are also enriched in short-chain organic acids like acetate (0.04 mM) and formate (0.1 mM), contributing ~20–30% of the dissolved organic carbon (DOC)[20], and in methanol (0.03 mM)[20,21]. The $\delta^{13}C$ of CH_4 (−37‰ to 2‰), acetate (−8‰), formate (4.8‰) and methanol (2.3‰) point to their abiotic formation[17,21]. While these serpentinization fluids sustain chemosynthetic life at the seafloor[22,23], the functioning and extent of the chemosynthetic microbial biosphere below the seafloor remains largely unknown. Cell counts in the serpentinite mud are variable, but overall low (10^1 to 10^6 cells cm^{-3})[20,24], presumably because of the

[1]Faculty of Geosciences, University of Bremen, Bremen, Germany. [2]Department of Geology & Geophysics, Woods Hole Oceanographic Institution, Woods Hole, MA, USA. [3]MARUM – Center for Marine Environmental Sciences, University of Bremen, Bremen, Germany. [4]Marine Chemistry and Geochemistry Department, Woods Hole Oceanographic Institution, Woods Hole, MA, USA. [5]Department of Geology, University of Innsbruck, Innsbruck, Austria. [6]Present address: Section of Geophysics, Alfred Wegener Institute, Helmholtz Centre for Polar and Marine Research, Bremerhaven, Germany. [7]Present address: MARUM – Center for Marine Environmental Sciences, University of Bremen, Bremen, Germany. ✉e-mail: pkumawat@uni-bremen.de

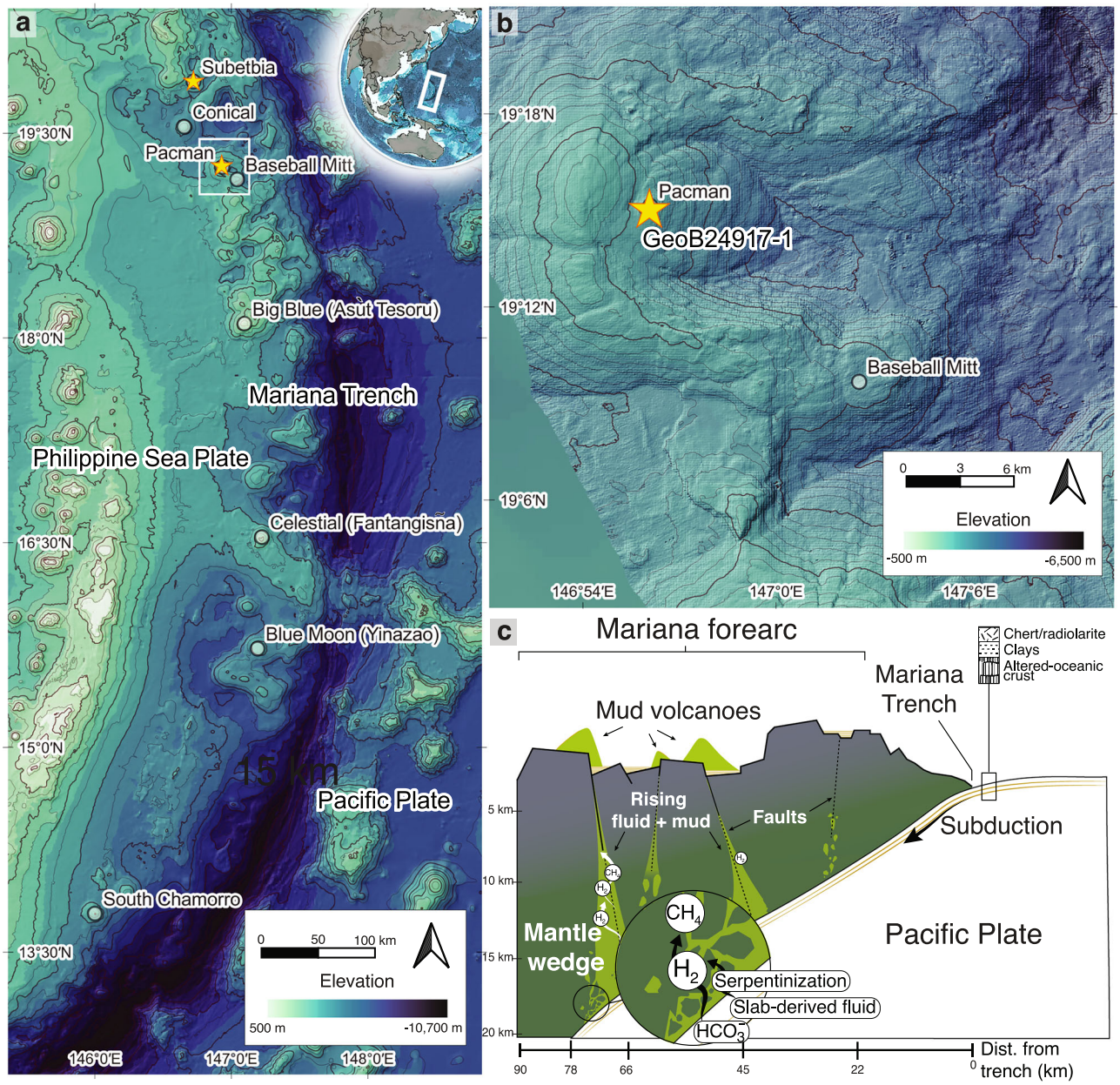

Fig. 1 | Study area and geological context of serpentinite mud volcanism in the Mariana subduction system. a Bathymetry map of the Mariana subduction system showing the incoming Pacific Plate, the overriding Philippine Sea Plate, the Mariana Trench, and a subset of the known serpentinite mud volcanoes on the forearc seafloor. Stars mark the locations of the Pacman and Subetbia mud volcanoes investigated in this study. Bathymetry from GEBCO Compilation Group[125]. **b** Bathymetry map showing the Pacman mud volcano and the location of gravity core GeoB24917-1 retrieved during expedition SO292/2. Bathymetric data collected during expedition SO292/2[26]. **c** Schematic of serpentinite mud volcano formation, following serpentinization of the mantle wedge by slab-derived fluids, formation of H_2 and CH_4, and the rise of serpentinite mud and fluids through deep-seated faults towards the seafloor.

high pH and intermittent fluid seepage[13,16]. Extremophilic archaea are believed to perform AOM as inferred from the detection of phospholipid-derived diphytanyl diethers and reduced sulfur species in the formation fluids[18]. Metabolic transcripts for denitrification and AOM were interpreted as evidence for nitrate-dependent AOM within the serpentinite mud volcanoes[24]. Although AOM is considered thermodynamically favorable here[19,25], direct evidence for AOM and its associated microorganisms is still lacking. Methanogenesis is a common metabolic strategy in serpentinization systems[13], but since CH_4 formation at the Mariana forearc is dominantly abiotic, the extent of microbial methanogenesis remains uncharacterized.

This study documents AOM coupled to sulfate reduction as a key metabolic process in the Mariana forearc, indicating the importance of methane cycling for the indigenous microbial community. Our findings also provide evidence of relict methanogenesis in the serpentinite mud, where its temporal distribution is possibly controlled by variable substrate availability. We present a comprehensive lipid biomarker and isotopic record from the Pacman and Subetbia mud volcanoes, providing insights into the habitability and survival strategies of extremophilic chemosynthetic life in this serpentinite biosphere.

Results and discussion

Geochemical and organic carbon transitions in serpentinite mud

The Mariana forearc hosts at least 19 active serpentinite mud volcanoes that root in a water-fluxed mantle wedge at a distance of ~30 to 90 km to the Mariana trench[15]. We investigated two sediment cores recovered during R/V *Sonne* expedition SO292/2[26] in 2022 (Fig. 1). Core GeoB24917-1 was

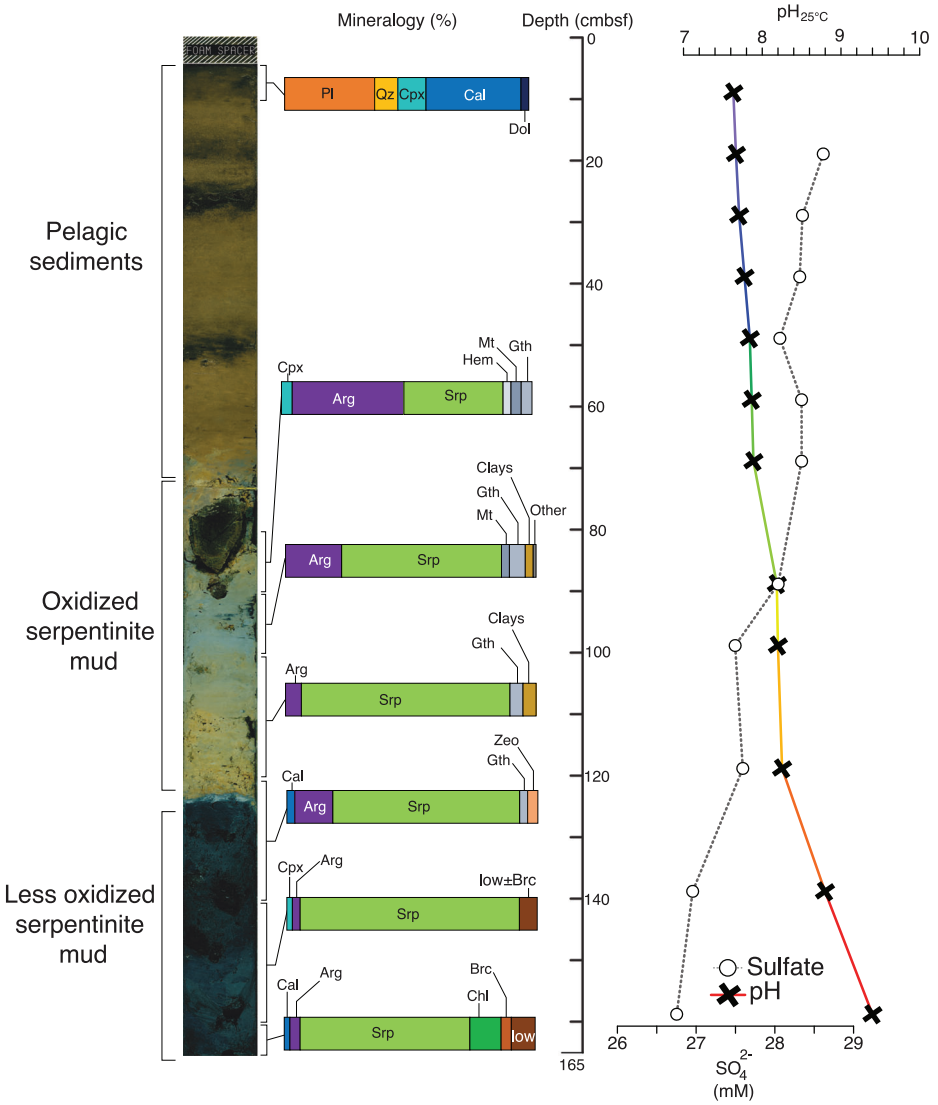

Fig. 2 | Lithology, mineralogy, and pore water geochemistry of core GeoB24917-1 (Pacman mud volcano). Lithological profile, mineral assemblages, and pore water pH (gradient line; top axis) and sulfate (dashed line; bottom axis) profiles from core GeoB24917-1 from the Pacman mud volcano summit. The mineral composition is based on XRD and thermogravimetry analyses. Arg aragonite, Brc brucite, Cal calcite, Chl chlorite, cmbsf cm below seafloor, Cpx clinopyroxene, Dol dolomite, Gth goethite, Hem hematite, Iow iowaite, Mt magnetite, Pl plagioclase, Qz quartz, Srp serpentine, Zeo zeolite.

recovered from the summit area of Pacman serpentinite mud volcano, located ~70 km west of the Mariana trench at 2997 m depth (Fig. 1a). The core extends to 165 cm below the seafloor (cmbsf) and is primarily composed of variably oxidized serpentinite mud, overlain by pelagic sediments (Fig. 2), offering an opportunity to study the transition from pelagic to serpentinite-hosted microbial communities. The bottom section (125–165 cmbsf) is deep blue in color and consists mainly of serpentine, with minor brucite and iowaite towards the bottom of this interval and aragonite at the top (Fig. 2, Supplementary Fig. 1, Supplementary Data 1). We interpret this section to represent serpentinite mud that is largely unaffected by seawater inflow. It is overlain by serpentinite mud, at 80–125 cmbsf, that is lighter blue-green in color and primarily composed of serpentine and aragonite. The lack of brucite in this topmost serpentinite mud suggests interaction with seawater during which brucite dissolved[27,28] and the mud was oxidized. We hereafter refer to this shallower layer of serpentinite mud as oxidized and to the bottom section as less oxidized. A summary of sampling intervals is listed in Supplementary Table 1.

The Pacman mud volcano fluids exhibit high pH (12.3) and low concentrations of SO_4^{2-} (13.9 mM)[17]. Pore water profile from our Pacman core shows a progressive increase from a seawater-like pH (7.6) at the core top to up to 9.4 at its bottom and a decrease in SO_4^{2-} concentrations from 28.6 to 26.8 mM (Fig. 2, Supplementary Data 2). These trends are indicative of seawater mixing with alkaline serpentinization fluids[17], although SO_4^{2-} can also be derived from the ascending serpentinization fluids, where the depletion in SO_4^{2-} concentrations with depth may in addition be attributed to microbial sulfate consumption[29].

Total organic carbon (TOC) contents in the serpentinite mud are low (<0.01 wt.%) with depleted $\delta^{13}C_{TOC}$ values (−31‰ to −28‰; Supplementary Table 2). These values are similar to those in high-pH horizons from other serpentinite mud volcanoes[20], and can be explained by the activity of chemosynthetic microorganisms that utilize ^{13}C-depleted dissolved inorganic carbon (DIC) ($\delta^{13}C$ range of −22.1‰ to 3.8‰[17,20]) or DOC ($\delta^{13}C$ range of −10‰ to −27‰[20]). On the contrary, TOC contents in the pelagic sediments are relatively higher (<0.02 to 0.04 wt.%) and exhibit $\delta^{13}C$ values consistent with a marine phototrophic origin ($\delta^{13}C_{TOC}$ of −21‰ to −20‰[30]; Supplementary Table 2).

The second core GeoB24930-1 was retrieved from the flank of Subetbia serpentinite mud volcano[26], on top of a major mudflow (Fig. 1a, Supplementary Fig. 2). The core is primarily composed of serpentinite mud, covered by <10 cm of pelagic sediment (Supplementary Figs 1, 3, Supplementary Data 1). Downcore pore water profiles are similar to those in the Pacman core but only reach a pH of 8.9 and SO_4^{2-} concentrations of <26 mM at the core bottom (272 cmbsf) (Supplementary Text 1.1, Supplementary Fig. 3, Supplementary Data 2).

Lipid biomarker zonation at Pacman mud volcano

To infer on the mud volcanoes' microbial community compositions, we investigated membrane lipids in the serpentinite mud. All cellular membranes are composed of intact polar lipids (IPLs) which provide a selectively permeable membrane between a cell and its environment. IPLs represent living or recently-active microbial colonies, as their polar head groups degrade after cell apoptosis[31]. Contrastingly, IPLs devoid of their polar head groups, i.e., core structures, have excellent preservation potential, making them favorable tools when investigating fossil communities[32]. Remarkably, intact and core membrane lipids reveal an abrupt change at the transition of pelagic sediment to serpentinite mud, indicating a shift in archaeal (Fig. 3a, b, Supplementary Data 3) and bacterial (Figs. 4a, b, 5a, c, 6a, Supplementary Data 4, 5) community composition with the changing geochemical environment. The chemical structures of all the lipids discussed in the text are illustrated in Supplementary Fig. 4.

The surface sediments are dominated by glycerol dialkyl glycerol tetraethers (GDGTs) present as core and intact forms with monoglycosidic (1 G) and minor amounts of diglycosidic (2G) headgroups bearing 0–3 cyclopentane rings (GDGT-3 only detected as core lipid). The sediments also show high abundances of core and intact crenarchaeol; a diagnostic marker for the water column dwelling *Thaumarchaeota*[33] (Fig. 3). In the topmost pelagic sediments, archaeal core lipids are twice as abundant as archaeal IPLs indicating low de novo production of IPLs and consequently lower microbial activity compared with the serpentinite mud, where archaeal IPLs are ~24 times more abundant than their core lipids (Fig. 3). Bacterial IPL concentrations are similarly low (<1 ng g^{-1}), consistent with low TOC (~0.04 wt.%). Despite their scarcity, bacterial IPLs are compositionally diverse, comprising mostly ester and ether-ester glycerol lipids with phospho- and amino headgroups (~90%), and minor occurrences of ether-based lipids (diethergycerol (DEG)) (Fig. 4, Supplementary Text 1.2, Supplementary Data 5). This observed archaeal and bacterial biomarker distribution is typical of a marine sedimentary community, where parts of the lipid material may be derived from water column[34–38]. These source assignments are consistent with their $\delta^{13}C$ values; −30 ± 2‰ to −24 ± 1‰ for archaeal tetraether lipids and −29‰ to −24‰ for bacterial-derived fatty acid chains (Supplementary Text 1.2, Supplementary Table 3).

The transition from pelagic sediment to serpentinite mud is marked by a shift in archaeal core and intact lipid biomarkers, from cyclic GDGTs and crenarchaeol to acyclic GDGT-0 and archaeal diethers (archaeol and hydroxyarchaeol). Archaeal IPLs increase in concentrations 30-fold to up to ~22 ng g^{-1} in the less oxidized zone, while archaeal core lipids remain at <3 ng g^{-1} throughout the serpentinite mud, indicating in-situ IPL production and heightened archaeal activity (Fig. 3c). Core and IPL inventories differ from each other in serpentinite mud, in higher diether/(diether +tetraether) lipid ratios for core lipids and point to, compositionally and temporally distinct archaeal populations, where core lipids are representative of past archaeal communities (Fig. 3d). Archaeol is produced by most archaea, including methanogens and methanotrophs, and is commonly reported from serpentinization-influenced marine[39–41] and terrestrial[42–45] sites, establishing it as a proxy for methanogenic organisms[46]. Hydroxyarchaeol synthesis is specific among methane-cycling archaea[46,47] and is typically attributed to methanotrophic archaea in environmental samples due to its strongly ^{13}C-depleted signature[48]. Among methanotrophic archaea, ANME-1 are known to produce glycosidic tetraethers and minor amounts of glycosidic diethers[49–51], making them plausible sources of both GDGTs and diether lipids observed in the serpentinite mud. A lack of cyclic GDGTs, typically associated with ANME-1[50,51], is striking and instead suggests methanogens as the source of GDGT-0 as they exclusively produce acyclic tetraethers[52]. Further details on the archaeal lipid distribution in the Pacman core are described in Supplementary Text 1.2.

Bacterial lipid distributions also shift downcore (Fig. 4). Phospho- and amino ester lipids are replaced by ether analogs, accompanied by an increase in sugar-based diether lipids (1G-DEG). Both core and intact DEGs exhibit increasing chain lengths and unsaturation with depth (Fig. 5, Supplementary Text 1.2). Core and intact DEG concentrations increase downcore from 8- and 3-fold respectively (from <2 ng g^{-1} to ~17 ng g^{-1} for core DEGs and ~6 ng g^{-1} for 1G-DEGs), reflecting in-situ sources. The synthesis of DEGs is typically understood as a membrane adaptation to environmental stress[53] or high temperatures[54], but when detected in AOM environments[48,50] and serpentinization-related sites[42–45,55] the occurrence of these lipids with diagnostic $\delta^{13}C$ values has been linked to the presence of SRB[53,54]. In our study, peak DEG concentrations observed at 100-120 cmbsf likely correspond to a zone of increased microbial activity of extremophilic bacteria, influenced by upward diffusion of reduced components into an oxygenated zone.

In addition to bacterial diether lipids, we also detected membrane-spanning branched GDGTs (Fig. 6, Supplementary Fig. 4), a class of non-isoprenoid tetraethers with a glycerol backbone and alkyl chains featuring methyl branching and cyclopentane moieties typically found in soil bacteria[56]. The deeper parts of the oxidized serpentinite mud (100–120 cmbsf) and the less oxidized serpentinite mud, exclusively show elevated concentrations (up to 5 ng^{-1}) of di-cycloalkylated branched GDGTs (Ic, IIc, IIIc), as well an additional presence of Overly Branched-GDGT IV (OB-GDGT-IV) and Sparsely Branched-GDGTs (SB-GDGT II and IV; Fig. 6a). A ~12-fold increase in concentration of these branched GDGTs relative to the pelagic sediments implies production of these lipids within the serpentinite mud by unidentified extremophilic bacteria (Fig. 6b).

Fate of methane in serpentinite mud: Evidence for methanotrophy

Ascending fluids at the Mariana forearc are enriched in CH_4 [17]. However, not all of this CH_4 escapes unaltered; some may be available for microbial consumption, leaving behind biochemical and isotopic signatures of methanotrophy. Measured $\delta^{13}C$ compositions of CH_4 from mud volcanoes range from −37‰ to 2‰[17]. The bulk $\delta^{13}C_{TOC}$ isotopic signatures we measured in pelagic sediments and serpentinite mud decrease downcore from −20‰ to −31‰, closely mirroring the $\delta^{13}C$ trends observed in lipids and reflecting shifts in microbial carbon assimilation pathways (Fig. 7a, Supplementary Tables 2, 3). Likewise, the combined $\delta^{13}C$ values of the core and intact lipid biomarkers show pronounced downcore shifts (Fig. 7a, Supplementary Tables 2, 3). Values for lipids in the less oxidized serpentinite mud drop to below −100‰, with values for hydroxyarchaeol of −106 ± 1‰, archaeol of −87‰, and GDGT-0-derived biphytane-0 of −104‰ at the core bottom. Such isotopic signatures can only be explained by the presence of methanotrophic communities and match previously reported $\delta^{13}C$ values from ANME-1 and ANME-2/−3 communities living in cold seep environments[49,50] (Fig. 7b). However, characteristic ANME-1 biomarkers, such as cyclic GDGT-1, −2, and −3[50,51], or even GDGT-4 in thermophilic ANME-1[57] were not detected in the serpentinite mud. Since the absence of these cyclic GDGTs is unexpected for a methanotrophic archaea, we suggest the preferential production of acyclic GDGTs by ANME-1 to be a response to environmental factors like pH, redox, and energy limitations (see below).

The presence of the ANME-1 community in less oxidized serpentinite mud suggests that elevated concentrations of DEGs originate from the sulfate-reducing partner bacteria in AOM. The detection of SRB-associated biomarkers suggests that microbial sulfate reduction may occur at a slow rate, which could explain the observed downcore depletion in pore water SO_4^{2-} concentrations (Fig. 2). Previous studies at the South Chamorro serpentinite mud volcano, assigned the depletion of SO_4^{2-} concentrations to microbial sulfate reduction under energy-limited, near-equilibrium conditions at ≥30 m below the seafloor[18,29]. Lipid biomarker investigations at South Chamorro determined the observed sulfate reduction to be enigmatically carried out solely by methanotrophic archaea involved in AOM, without having found the common phospholipid fatty acids of SRB[18,58]. Our data confirms the absence of substantial amounts of fatty acid-based polar lipids and instead shows shifts in bacterial membrane compositions from ester to ether lipids. This highlights that fatty acid-based approaches do not provide a holistic picture of microbial communities in such environments. The ^{13}C-depletion in DEGs in the deepest sample ($\delta^{13}C$ of −74 ± 7‰ to

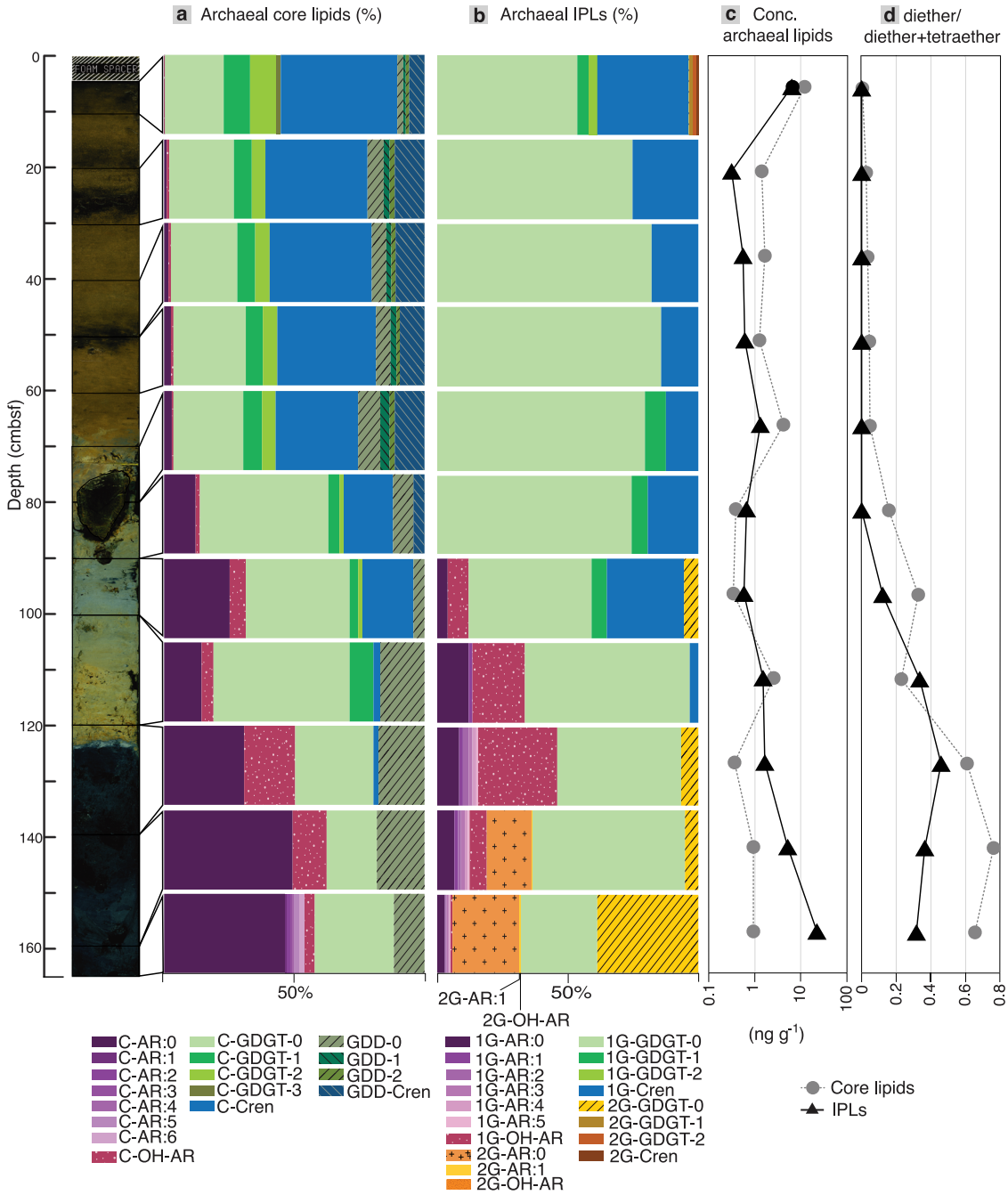

Fig. 3 | Downcore archaeal lipid biomarker distribution for core GeoB24917-1 (Pacman mud volcano). Relative abundances of various archaeal core (C-) lipids (**a**) and archaeal IPLs (**b**) detected in pelagic sediments and serpentinite mud. We observe a shift from dominantly marine water column and marine detrital lipid biomarkers in pelagic sediments to a mixed methanotrophic and methanogenic signal in serpentinite mud. GDDs transition from a mixed (GDD-1, −2, -crenarchaeol) to an acyclic form (GDD-0) further suggesting a preferential production of acyclic GDGTs in the serpentinite mud. **c** Absolute concentrations of archaeal core lipids (dashed grey line; grey bullets) and IPLs (solid black line; filled black triangles) showing increase in archaeal IPL concentrations within less oxidized, i.e., dark blue, serpentinite mud. **d** Ratio of diether lipids (AR + OH-AR) to diether lipids + tetraether lipids (GDGTs) for core (dashed grey line; grey bullets) and intact polar lipids (solid black line; filled black triangles) suggesting an increase in abundance of core diether lipids in the less oxidized serpentinite mud. AR archaeol, cmbsf cm below seafloor, Cren crenarchaeol, GDD glycerol dialkyl diether, GDGT glycerol dialkyl glycerol tetraether, IPL intact polar lipid, OH-AR hydroxyarchaeol.

−57‰; Fig. 7a) underlines the presence of SRB involved in AOM[49,50,59]. We assign the ^{13}C-depletion in DEGs to lithotrophic sulfate reduction in a system open to resupply of DIC[60]. This complies with the high $\sum CO_2$ concentrations measured in fluids, with $\delta^{13}C_{DIC}$ of −22.1‰ to −3.8‰ from neighboring mud volcanoes[18]. Given the known carbon isotopic fractionation between substrate and lipids for lithotrophic sulfate reduction[61], the measured $\delta^{13}C$ of DEGs is ~10‰ lighter than the expected range of −64 ± 3‰ to −47 ± 2‰ based on reported $\delta^{13}C_{DIC}$ values (Supplementary Table 4). The DEGs at 140-160 cmbsf show a $\delta^{13}C$ range of −59 ± 5‰ to −38‰ (Fig. 7a), well within the expected range for lithotrophic sulfate reduction. This suggests that SRBs at ANME-dominated depth (160-165 cmbsf) likely utilize an additional isotopically depleted carbon source alongside DIC.

A previous study[24] identified sulfate reduction transcripts in serpentinite mud, but proposed that AOM in the mud volcanoes is primarily coupled to denitrification. Denitrifying AOM can occur via consortia of nitrate-

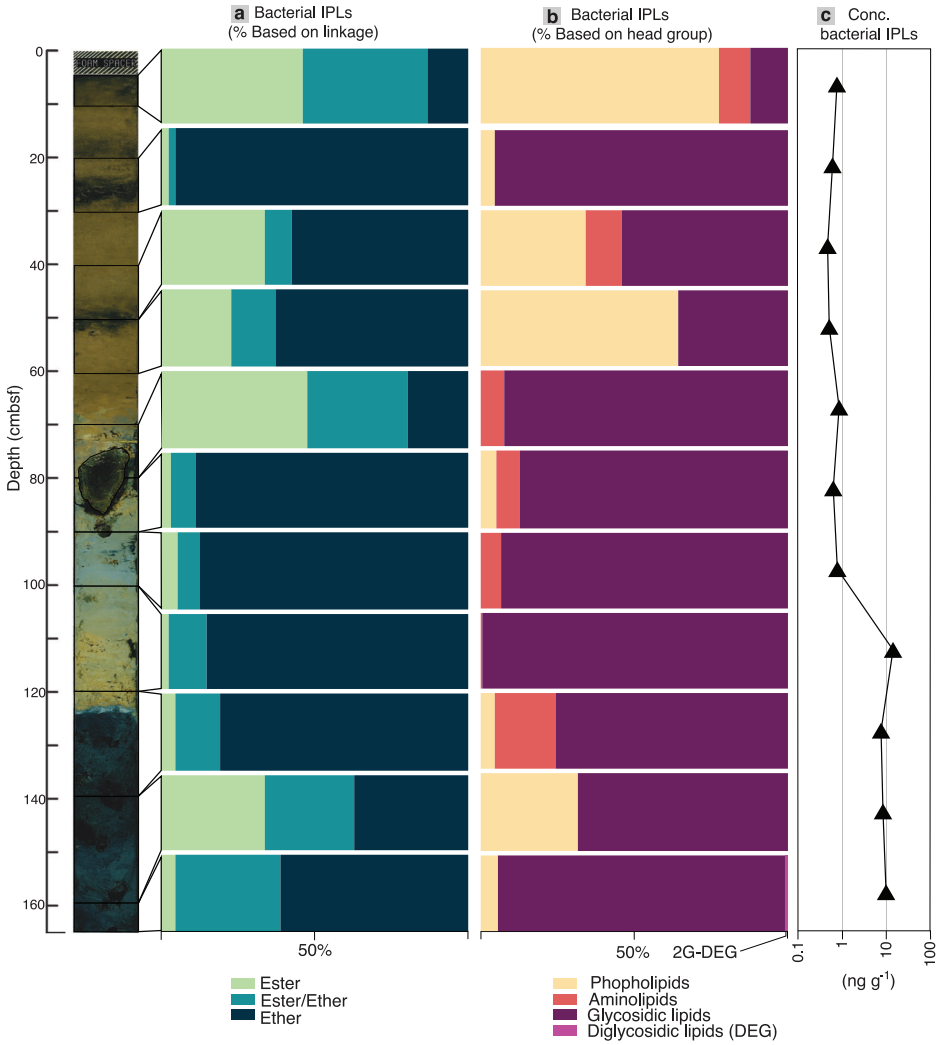

Fig. 4 | Downcore bacterial lipid distributions for core GeoB24917-1 (Pacman mud volcano). **a** Relative abundances of various bacterial IPLs, as based on their structural linkages. Note the dominance of ether lipids within serpentinite mud. **b** Relative abundances of various bacterial IPLs based on their head groups. Glycosidic lipids dominate within serpentinite mud. **c** Absolute concentrations of bacterial IPLs showing an increase in bacterial IPL concentrations within serpentinite mud. cmbsf cm below seafloor, DEG diethergly-cerol, IPL intact polar lipid.

reducing ANME-2d archaea or ANME-2d archaea paired with anammox bacteria[62–64], and are typically found in freshwater environments and have not been observed in consortia with SRB[65]. We cannot entirely exclude this scenario, but it seems unlikely. Despite the higher energy yields of nitrite/nitrate-dependent AOM compared with sulfate-dependent AOM[66], denitrifying AOM is uncommon in subseafloor environments. Nitrate and nitrite are rapidly depleted in water column and their concentrations continue to decrease within the sediments[67], and are not expected to be abundant in serpentinizing fluids. Moreover, computing Gibbs free energies ($\Delta_r G$) at in-situ conditions (2 °C, 300 bar, pH 10) demonstrates that autotrophic sulfate reduction is feasible, with a $\Delta_r G$ of −179.3 kJ mol^{-1} (Supplementary Table 4), and when coupled with AOM, is an exergonic catabolic pathway (−66.6 kJ mol^{-1}). Based on the observed coupling of isotopically depleted diagnostic SRB markers with an ANME-1 signal and the high energy yields of sulfate reduction, we conclude that sulfate-dependent AOM is the most likely scenario within the serpentinite mud.

Molecular traces of relict methanogenesis in serpentinite mud

The ^{13}C-depleted signature typical of ANME lipids is less pronounced at 140-160 cmbsf (Fig. 7a), where biphytane-0, archaeol, and hydroxyarchaeol exhibit δ^{13}C values of −73 ± 3‰, −65 ± 1‰, and −92‰, respectively (Supplementary Table 3). The ^{13}C-depleted hydroxyarchaeol suggests an ANME origin, but the relative ^{13}C-enrichment in archaeol, and especially biphytane-0 indicate contributions from other sources, potentially heterotrophic archaeal communities. Assuming heterotrophy-associated δ^{13}C composition for biphytanes-0 (−26‰; 0-10 cmbsf) and archaeol (−29.4‰[68]), ~40% of the biphytane-0 and 38% of archaeol needed to be derived from the heterotrophic archaea to explain the observed mixed isotopic signal. However, the low TOC contents in the serpentinite mud and archaeol abundances of ≤3% in the overlying sediments make this scenario appear unlikely, although possible admixes from these sources cannot be ruled out. Alternatively, the heavier isotope signals at 140-160 cmbsf reflects input from chemoautotrophic communities such as methanogenic archaea, known to produce structurally similar lipids (e.g., [39,55]). The presence of methanogenic archaea in the sulfate-reduction zone, however, would be unusual as SRB typically outcompete methanogens for H_2 consumption, given the higher energy yield of sulfate reduction over CO_2 reduction[69]. Despite this, such coexistence has been observed in the Lost City carbonate chimneys and Chimaera seeps where H_2 supply (up to 15 mM[70]) may support their co-occurrence[42,55]. At Lost City, SRB might be utilizing abiogenic formate, while methanogenic archaea engage in autotrophic methanogenesis[71]. However, under high H_2 and CO_2 conditions, formate-based sulfate reduction is unlikely, as elevated H_2 inhibits hydrogenase enzyme activity and thermodynamically shifts formate disproportionation toward formate production, suppressing its consumption[72,73]. We therefore conclude that this co-occurrence is only conceivable if methanogenic archaea utilize alternative substrates such as formate, acetate, methanol or non-competitive substrates such as methylated amines, given the relatively low H_2 concentrations (≤1 mM[20]) compared to the Lost City hydrothermal fluids[12,70].

To assess potential methanogenic contributions diluting ANME-derived lipid δ^{13}C signals, we applied an isotope mass balance

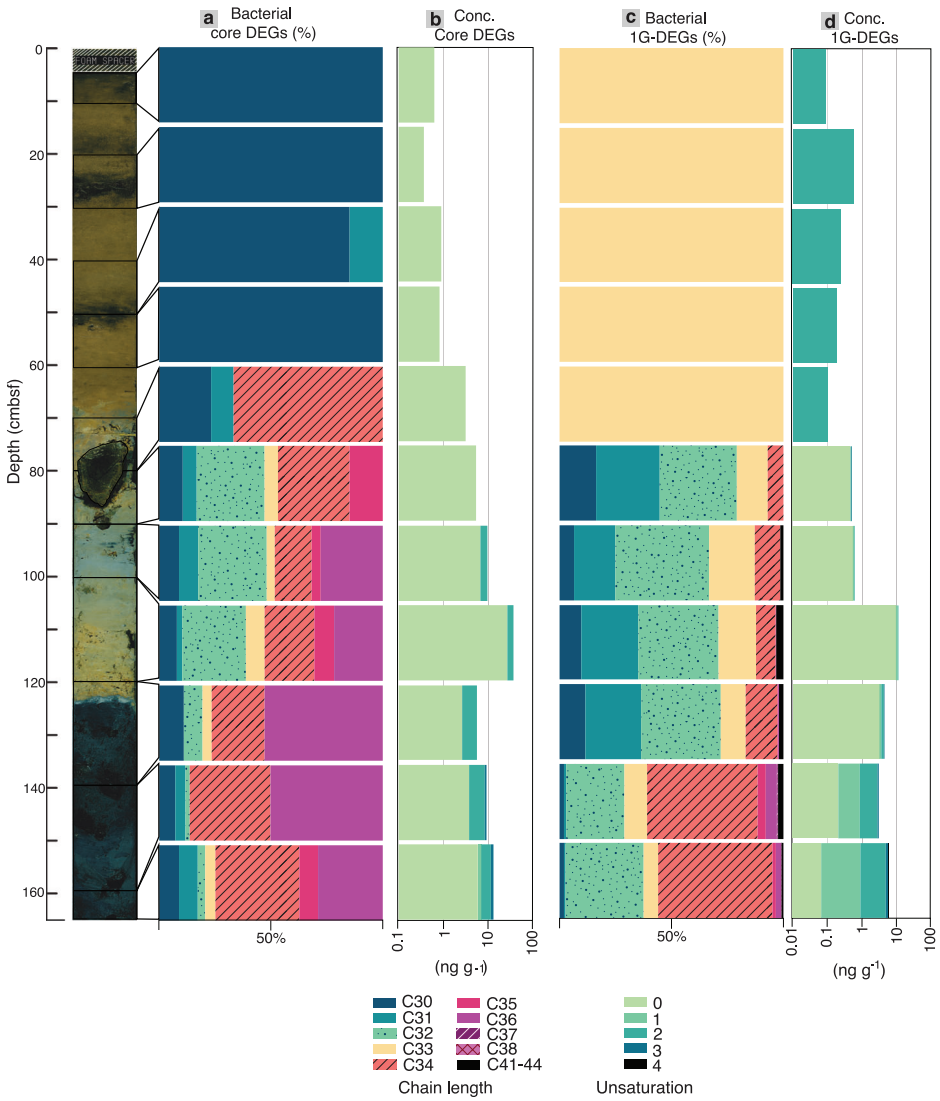

Fig. 5 | Downcore bacterial diether lipid structural variations for core GeoB24917-1 (Pacman mud volcano). Relative abundances of bacterial C-DEGs show increased chain length (**a**) and (**b**) increased degrees of unsaturation as well increased C-DEG concentrations within serpentinite mud. Trends in relative abundances of bacterial 1G-DEGs, exhibiting increases in chain length (**c**) and (**d**) increases in degree of unsaturation, as well as increases in 1G-DEG concentrations within serpentinite mud. cmbsf cm below seafloor, DEG dietherglycerol.

(Supplementary Methods 2.1, Eqs. 1, 2), estimating $\delta^{13}C$ ranges using known fractionation patterns[74] and calculating the minimum and maximum methanogenic inputs needed to explain the mixed values (Supplementary Fig. 5, Data 7). Methanogenic archaea are known to exhibit a broad $\delta^{13}C$ range due to their use of diverse carbon substrates (CO_2, acetate, methylated compounds), each with distinct isotopic signatures[74,75]. Our results suggest that hydrogenotrophic (at high H_2), acetoclastic, and methanol-dependent methanogenesis best account for this dilution due to their modest carbon isotopic fractionation[74]; with methanogenic archaea contributing 26-41% of archaeol (excluding high methanol condition), 13–22% of hydroxyarchaeol, and 34% of biphytane-0 (only acetoclastic methanogenesis) at 140–160 cmbsf. Although $\Delta_r G$ for each pathway is exergonic at in-situ conditions (Supplementary Data 7), methanol-dependent methanogenesis is the most energetically favorable pathway (-248.3 kJ mol^{-1}), followed by hydrogenotrophic methanogenesis (-112.8 kJ mol^{-1}) whereas acetoclastic methanogenesis (-24.9 kJ mol^{-1}) barely surpasses the minimum biological energy quantum[76]. Likewise, the modest carbon isotopic fractionation associated with methylotrophic methanogenesis (trimethylamine; under limited abundance)[74] could contribute to isotopic dilution in the serpentinite mud. However, this pathway is unlikely to proceed in biomass poor mud volcanoes, where methylated substrates typically require sufficient organic precursors[77,78]. Formate-dependent methanogenesis is suggested as an adaptive metabolic pathway in high pH and DIC limited environments[79,80], where the high concentrations of abiotically produced formate in the ascending mud volcano fluids come with notable energy yields (-90 kJ mol^{-1}) for this pathway. Genomic markers[81,82] and knowledge of isotopic fractionation during formate-dependent methanogenesis are required to test if this metabolic pathway is favorable in serpentinite mud volcanoes.

Regardless of the specific substrate utilization pathways, the co-occurrence of methanogenic archaea and SRB at the Mariana forearc requires an alternative substrate for methanogenic archaea to remain competitive. In marine sediments, the methanogenic zone typically underlies the zone of coupled sulfate-reduction and methane oxidation[65,83]. We propose that a formerly active group of methanogenic archaea is responsible for the observed heavier isotope signal for biphytane-0, archaeol and hydroxyarchaeol. This is supported by shifts in core diether lipid abundances in serpentinite mud, where the ratio of diether/(diether + tetraether) for core archaeal lipids is ~1.8 times greater than that of archaeal IPLs (Fig. 3d). But core lipid concentrations alone are insufficient to account for this dilution, suggesting additional input from the IPL pool. Considering the slow degradation rates of glycosidic ether lipids in marine sediments[35], a considerable fraction of the IPLs could also carry a relict isotope signal of a now inactive community.

Hydrogenotrophic methanogenesis is common in serpentinization systems[13,42,71], and the detection of [NiFe]-hydrogenase genes indicates that this metabolic strategy is also used in the serpentinite mud volcanoes of the Mariana forearc[24]. The ^{13}C-enriched values for archaeol and

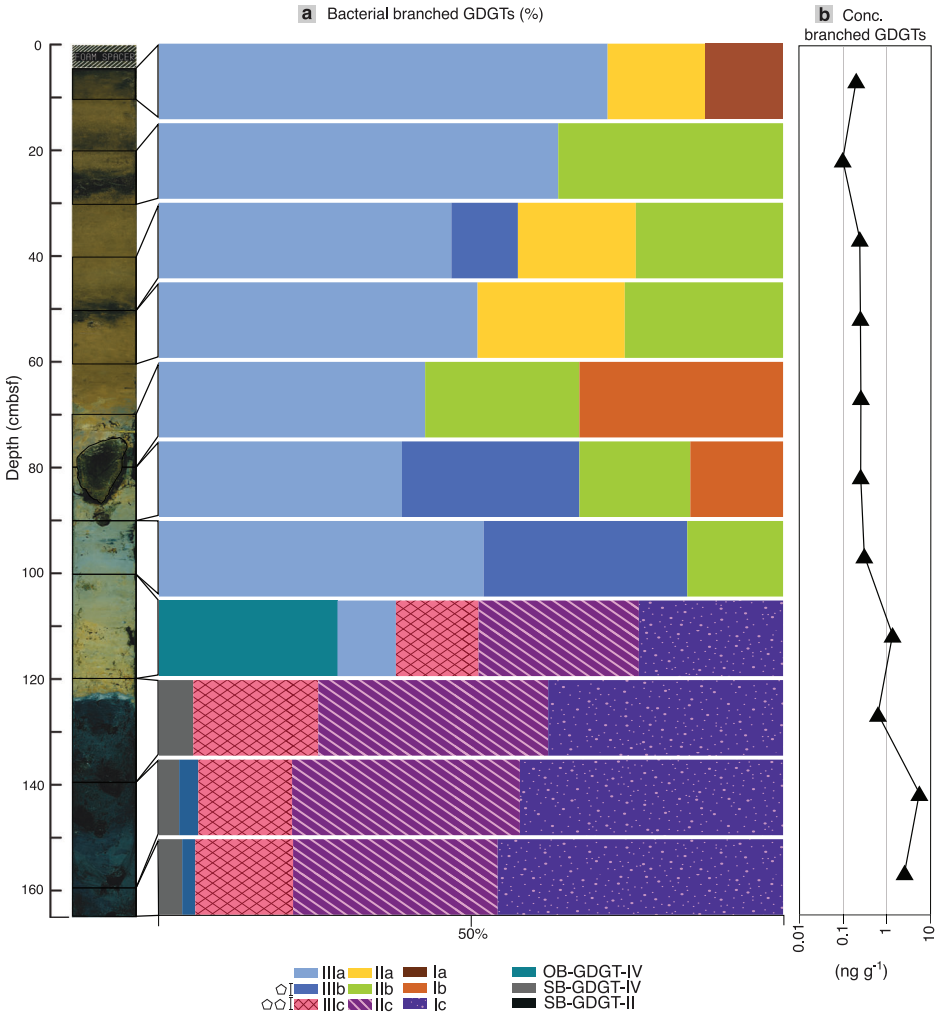

Fig. 6 | Downcore variations of bacterial branched GDGTs for core GeoB24917-1 (Pacman mud volcano). a Relative abundances of branched GDGTs, showing a shift from dominantly acyclic and monocyclic branched GDGTs with variable methyl groups in pelagic sediments to a dominance of branched GDGTs with two cyclopentane rings and variable methyl groups in serpentinite mud. **b** Absolute concentrations of branched GDGTs (solid black line; filled black triangles), displaying increased abundances within serpentinite mud.cmbsf cm below seafloor, GDGT glycerol dialkyl glycerol tetraether, OB overly branched, SB sparsely branched.

hydroxyarchaeol (−27‰ and −26‰, respectively) at Subetbia mud volcano provide additional evidence for hydrogenotrophic methanogenesis (Fig. 8). These values align with expected $\delta^{13}C$ values for hydrogenotrophic methanogenesis under high H_2 conditions (Fig. 8b). At 260-272 cmbsf in this core from Subetbia, archaeal diethers, both core and IPLs constitute ~99% of the total archaeal lipid pool (Supplementary Fig. 6). A near absence of GDGTs (<1% of the total archaeal lipid pool) at this depth suggests minimal overprinting by AOM, preserving a pristine methanogenic biomarker signal within serpentinite mud. Moreover, the combination of ^{13}C-enriched diether lipids with similar core and intact archaeal lipid concentrations (0.9 ng g^{-1} each) supports the presence of an unmasked relict signal of hydrogenotrophic methanogenesis at Subetbia. Additional details on archaeal and bacterial biomarker zonation in the Subetbia core are provided in Supplementary Text 1.3 and Supplementary Figs. 6,7.

Notably, the $\delta^{13}C$ of archaeal diether lipids at Subetbia mud volcano and the calculated $\delta^{13}C$ range for methanogenic lipids at Pacman are more ^{13}C-depleted than those from other serpentinization sites[42,55] (Fig. 8a). At a measured pH of ~10 in the serpentinite mud, a substantial portion of DIC remains available for microbial uptake (Supplementary Fig. 8). Cool serpentinization fluids are usually DIC depleted because calcium carbonate precipitates under hyperalkaline conditions[13,84]. At Lost City and Chimaera, the unusual ^{13}C-enrichment of methanogenic archaeal lipids is attributed to carbon limitation[42,55], which leads to minimal isotopic discrimination[55,74] and ^{13}C-enriched diether lipids (Fig. 8a). At the Mariana forearc, however, a substantial amount of carbon is delivered to and subducted at the Mariana trench[85,86], which is mobilized from the slab[87] and transported back to the seafloor through mud volcanism[17,18]. As these fluids ascend, most DIC is reduced to CH_4[17], but considerable amounts of DIC (up to 40 mM[17,18]) may persist. The mud volcano fluids hence, show DIC concentrations considerably higher than what has been measured at Lost City (up to 26 µM). Therefore, carbon limitation is unlikely to constrain the subseafloor biosphere in the Mariana forearc. Moreover, low cell counts in the serpentinite mud[18,20,24] suggest minimal competition for substrates, indicating that these microbial communities are constrained by high pH, nutrient limitation, and fluctuating substrate availability rather than carbon availability. This likely enables microbial communities to discriminate between ^{12}C and ^{13}C, as evidenced by the comparably depleted archaeal diethers in the mud volcanoes compared to other serpentinization ecosystems.

Although much of the CH_4 in the Mariana forearc is produced abiotically, this study provides biomarker evidence for localized biogenic CH_4 production, consistent with light $\delta^{13}C_{CH4}$ (−80‰) at the South Chamorro[17]. Our biomarker data from Pacman suggest a transition from a relict methanogenic community to a later AOM-dominated community within the brucite and iowaite bearing-serpentinite mud, reflecting shifts in community composition driven by transients in substrate availability that relates to episodic ascent of serpentinization fluids. We hypothesize that hydrogenotrophic methanogenic archaea thrive in H_2-rich serpentinization fluids but when H_2 concentrations decrease, sulfate-reducing bacteria take over[88] (Fig. 9). This biological regime shift may be explained by the geochemical changes that accompany the upward migration of serpentinite mud. We propose that the upward migration of serpentinite mud through the forearc crust exposes it to increasing seawater-derived SO_4^{2-}, establishing a redox gradient that favors sulfate-dependent AOM over methanogenesis. This transition establishes a redox gradient in which sulfate-dependent AOM

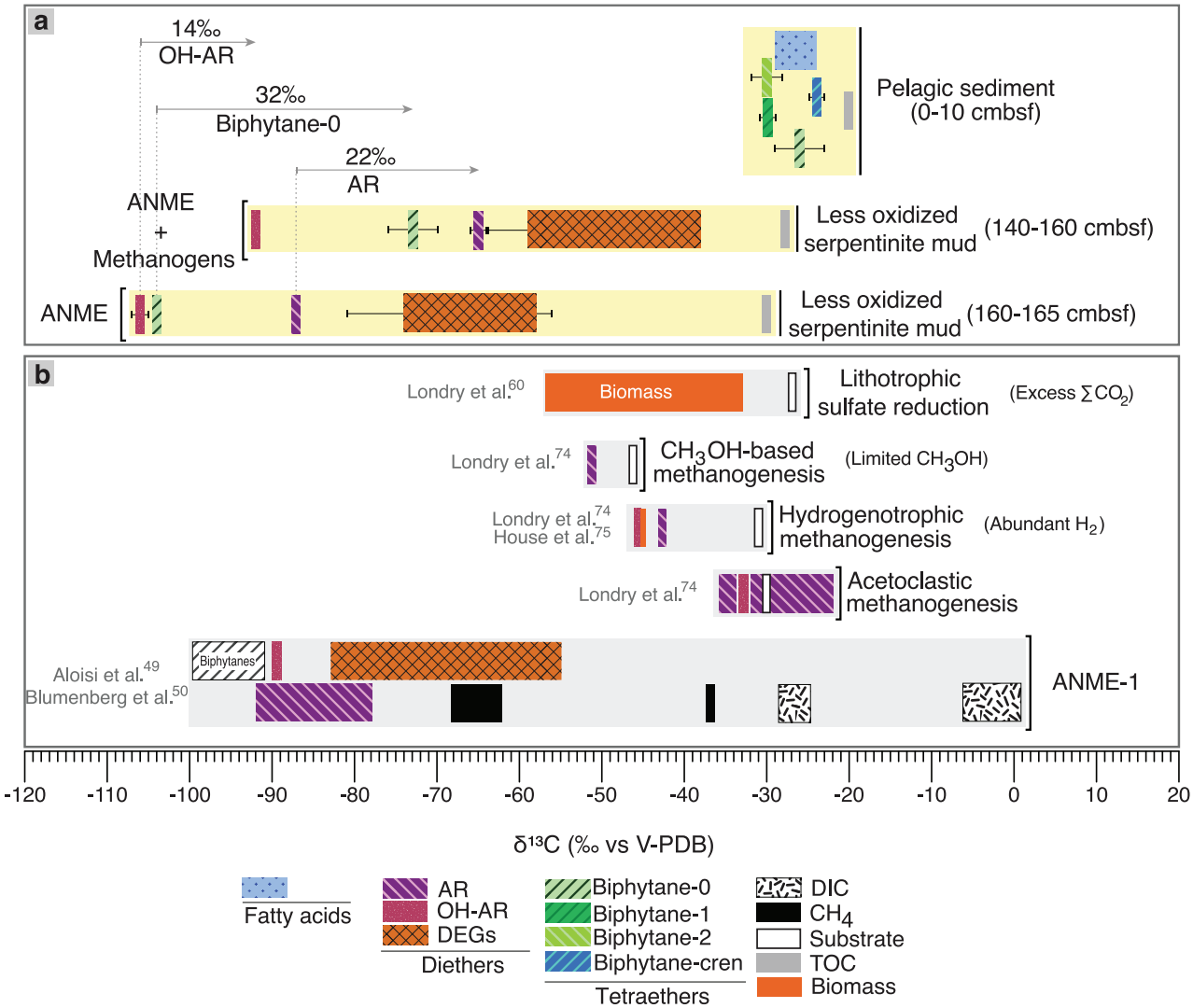

Fig. 7 | Compound-specific $\delta^{13}C$ compositions of diagnostic lipid classes. Compound-specific $\delta^{13}C$ compositions of various diether and tetraether lipids from **a** Pacman mud volcano (yellow shaded boxes) compared to isotopic compositions observed in various **b** environmental and lab cultures (grey shaded boxes), as well as $\delta^{13}C$ values for DIC, CH_4, TOC, and substrates. Error bars in (**a**) show the maximum and minimum deviation from the mean $\delta^{13}C$ values for individual compounds based on replicate measurements for each sample. Error bars for $\delta^{13}C$ ranges of DEG compound classes represent the deviation from the mean $\delta^{13}C$ maxima and minima for the given range. All $\delta^{13}C$ values and respective errors are reported in ‰ relative to the V-PDB standard. ANME anaerobic methanotrophic archaea, AR archaeol, cmbsf cm below seafloor, Cren crenarchaeol, DIC dissolved inorganic carbon, OH-AR hydroxyarchaeol, TOC total organic carbon, V-PDB Vienna-Pee Dee Belemnite.

becomes thermodynamically more favorable than methanogenesis, creating an ecological advantage for methane-oxidizing communities. Thus, the overprinting of methanogenic lipid signatures by AOM-associated compounds likely reflects a depth-dependent reorganization of microbial metabolism in response to progressive oxidation of the system during mud ascent.

Microbial adaptations to high alkalinity and nutrient limitation

For microbial life to adapt to alkaline and reducing conditions and nutrient scarcity in serpentinization systems, its cell membrane is the first line of defense. Membrane lipid remodeling by modifying IPL compositions preserves integrity and function[89–91]. In the microbial communities of Mariana mud volcanoes, increased transcripts that are linked to membrane maintenance emphasize the significance of this strategy[24].

Replacing ester lipids with ether lipids seems to be a common strategy among extremophilic bacteria[92,93]. At Pacman, the shift from ester- to ether-based IPLs in serpentinite mud with changing geochemistry allows extremophilic communities to thrive, possibly reducing membrane repair needs[89], adapting to energy deprivation[36], anoxia[53], redox[94] and/or high pH[90]. Furthermore, the preference for ether-based glycolipids (1G-, 2G-DEG) over ester/ether-based phospholipids suggests adaptation to phosphate limitation[95], as alkaline fluids prevent Ca-phosphate leaching[96]. Available phosphate is likely scavenged by brucite[97], which is abundant in serpentinite mud[87]. Preferential glycolipid production may help counteract high ion gradients[98], as their hydroxyl-rich headgroups allow dense membrane packing facilitated by hydrogen bonding, preventing water-mediated swelling under ionic stress[99]. These adaptations likely enable bacteria to maintain membrane stability and function.

A preferential synthesis of additional sugar groups (2G-AR, 2G-GDGT-0) among membranes of ANME-1 archaea may indicate adaptation to nutrient and energy stress[38,100]. A direct link to phosphate availability has not been shown in cultures, but preferential 2G-GDGT production has been associated with energy limitations and dormancy[101], suggesting substrate exhaustion in serpentinite mud pore waters. However, abundant H_2 and CH_4 in Mariana mud volcano fluids[17,20] in connection with low cell counts imply that these microbial communities are rather challenged by factors other than substrate availability, such as high pH. GDGT production likely enhances membrane stability by reducing permeability[89], a crucial

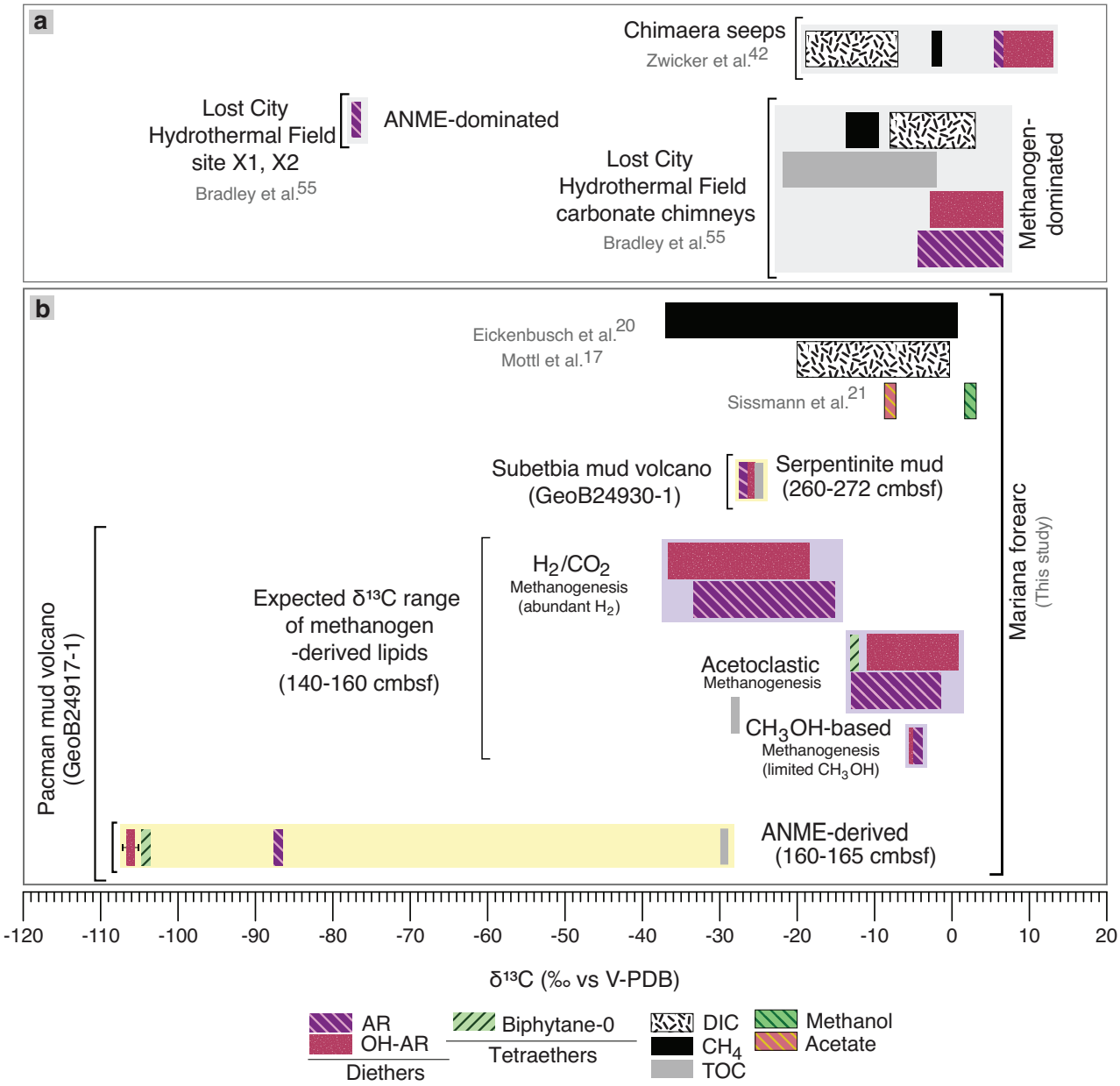

Fig. 8 | Isotopic composition of archaeal lipids in serpentinization ecosystems, carbon species and substrates. a Compound-specific $\delta^{13}C$ isotopic composition of archaeal lipids at Chimaera seeps and Lost City hydrothermal vent field (grey shaded box). **b** Compound-specific $\delta^{13}C$ isotopic composition of ANME-derived lipids at Pacman mud volcano (yellow shaded box), expected compound-specific $\delta^{13}C$ isotopic range of methanogen-derived lipids for various methanogenic pathways based on the known isotopic substrate-to-lipid fractionation and known substrate $\delta^{13}C$ composition at Mariana forearc (purple shaded boxes). Compound-specific $\delta^{13}C$ isotopic composition of archaeal diethers detected in core GeoB24930-1 at Subetbia mud volcano (yellow shaded box). All $\delta^{13}C$ values are reported in ‰ relative to the V-PDB standard. ANME anaerobic methanotrophic archaea, AR archaeol, cmbsf cm below seafloor, DIC dissolved inorganic carbon, OH-AR hydroxyarchaeol, TOC total organic carbon, V-PDB Vienna-Pee Dee Belemnite.

adaptation for extreme acidophiles and alkaliphiles[102,103]. The tolerance of ANME-1 archaea to high salinity[104] may also favor their presence in such an alkaline environment. The exclusive production of GDGT-0 may reflect a unique response to high pH through reduced cyclization, although other factors like temperature and reducing conditions also play a role[94,105,106].

We observed an increased chain unsaturation in archaeal and bacterial membrane lipids within the serpentinite mud (Figs. 3, 5, Supplementary Figs. 9, 10, 11). In less oxidized sections, core and intact archaeol exhibit unsaturation. Archaeol with up to six double bonds comprises ~13% of the total core diether lipids. Unsaturated 1G-AR with up to five double bonds are found throughout the serpentinite mud, constituting up to 5% of the total archaeal IPL diethers. Chain unsaturation is common among halo(alkali)philic[107] and psychrotrophic archaea[108], helping maintain membrane fluidity and reducing leakage under salinity and cold stress. Similarly, bacteria increase unsaturation in DEGs, where unsaturated 1G-DEGs (up to three unsaturations) range from 10-16% in oxidized and 27–98% in less oxidized mud (where also up to four unsaturations were found) (Fig. 5). Similarly, unsaturated core DEGs (up to four unsaturations) dominate the total core DEG pool (53–58%) in the less oxidized serpentinite mud. This increase in unsaturation is accompanied by an increase in chain length, despite the fact that unsaturated shorter chains are typically favored in cold environments[90]. In a highly alkaline and cold environment, however,

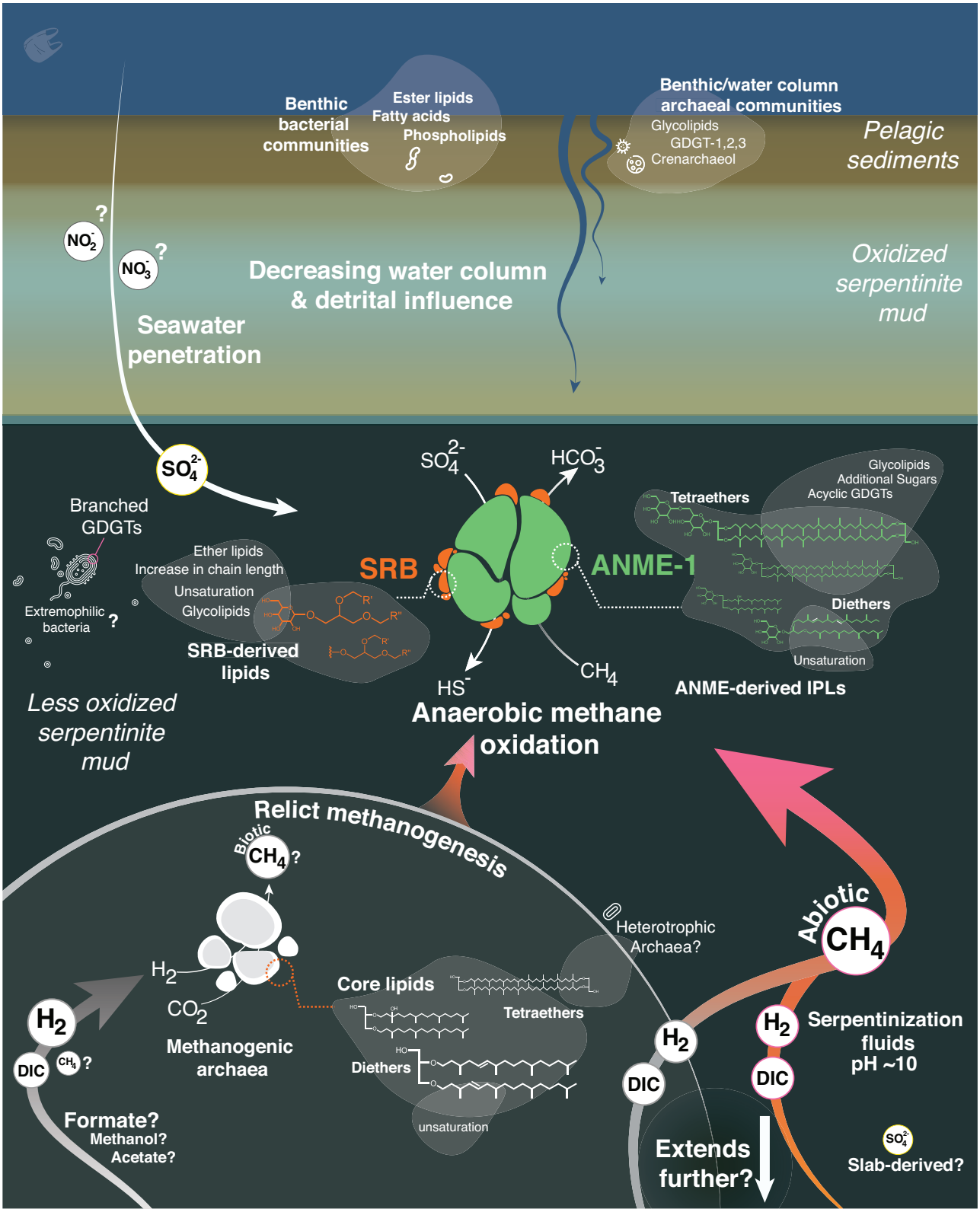

longer unsaturated bacterial diether lipids synthesis may reflect a compensatory mechanism where longer diether chain length reduces membrane permeability to prevent disruptive hydroxyl ion flux and increase membrane stability, as observed among archaea[107,109]. Unsaturated diether lipids have been reported in methanogenic archaea from serpentinite-hosted seeps[44], but appear to be absent in alkaline systems venting at higher temperatures[12,39]. This suggests that lipid unsaturation likely reflects an adaptation to environments where alkaline fluids remain cool.

Tetraether lipids are key membrane adaptations in archaea under high ion strength environments[102]. Similarly, branched GDGTs can enhance bacterial membrane stability[110]. The latter have been described from diverse terrestrial and marine environments[40,43,111,112]. Their high concentrations in

Fig. 9 | Schematic of microbial succession and biogeochemical processes in serpentinite mud at the Mariana forearc. This schematic depicts lipid biomarker transitions from pelagic sediment communities to extremophiles adapted to high pH and redox conditions in serpentinite mud. The Mariana forearc biosphere is fueled by alkaline serpentinization fluids enriched in H_2, CH_4, DIC, and organic acids, sustaining specialized microbial communities. Lipid and stable carbon isotope data reveal a shift from relict methanogenic archaea, likely engaged in hydrogenotrophic methanogenesis, to a later ANME-SRB community mediating anaerobic oxidation of methane (AOM). Changes in substrate availability likely drove this transition. Distinct lipid signatures, including unsaturated diethers, acyclic GDGTs, and ether-based glycolipids, highlight adaptations to pH stress, phosphate limitation, and fluctuating redox conditions. The presence of in-situ branched GDGTs suggests previously uncharacterized bacterial communities persisting in these ultra-oligotrophic conditions. The Mariana forearc serpentinite biosphere, shaped by episodic fluid flow and substrate shifts, provides insights into deep-sea subsurface habitability. DIC = dissolved inorganic carbon, ANME anaerobic methanotrophic archaea, SRB sulfate-reducing bacteria, AOM anaerobic oxidation of methane, GDGT glycerol dialkyl glycerol tetraether.

the less oxidized sections suggest in-situ production by unknown alkaliphilic bacteria. Increased cyclization may help bacteria adapt to high pH[113,114], while elevated concentrations downcore could indicate responses to anoxic and reducing conditions[115], at which these bacterial ether-based lipids offer a low oxidation state of carbon[94]. Additionally, methyl groups may also mitigate cold stress by maintaining membrane fluidity[90,113]. These lipids, once seen as soil proxies[56], now stand as a testament to bacterial ingenuity, showcasing their critical role in membrane adaptation to extremophilic niches. These results reshape our understanding of biomarkers for life's adaptation and evolution in harsh environments.

Summary & conclusions

Our findings provide foundational understanding of the subsurface serpentinite-hosted biosphere in the Mariana forearc. The lipid biomarker transitions from pelagic sediment into serpentinite mud highlight the resilience of microbial communities, finely tuned to shifting geochemical gradients, with extremophiles becoming dominant as conditions deviate from pelagic sediment norms (Fig. 9). Unsaturation among diethers, dominance of acyclic GDGTs, and ether-based glycolipids suggest an adaptive strategy to stabilize membranes under alkaline and phosphate-limited, reducing and energy-limited conditions. The in-situ production of distinct branched GDGTs underscores the role of methyl branching and internal cyclization in microbial adaptation within this environment. Our stable carbon isotope data and biomarker distributions within the brucite and iowaite-bearing serpentinite mud reveal a dynamic history of microbial activity, from early (likely hydrogenotrophic) methanogenesis to subsequent sulfate-dependent AOM (only at Pacman) and other extremophilic bacterial communities. Our data suggest that diverse metabolic pathways in this system are shaped by dynamic geochemical conditions, fluctuating redox states, and the availability of energy-rich substrates such as H_2 and CH_4, allowing extremophilic microorganisms to persist in a slow-turnover state.

Low cell counts and low biomass make DNA extractions in this habitat challenging. Coupling of lipid biomarkers and carbon isotopes proves useful in providing reliable insights into microbial processes in such ultra-oligotrophic environments. The Mariana forearc hosts a sparsely populated, yet extraordinary biosphere. Our findings just scratch the surface of this habitable zone, where the cool nature of the hydrated mantle wedge and abundant supply of electron donors and acceptors potentially enable this biosphere to extend far beneath the seafloor, remaining within the thermal limits of life[16,116]. The Mariana forearc biosphere emerges as a distinct endmember among serpentinite-hosted ecosystems, differing in terms of episodic substrate and carbon availability. Unraveling these dynamic serpentinization-hosted habitats deepens our understanding of subsurface habitability on Earth and provides valuable insights for exploring the potential for life in the Solar System.

Methods

Sampling and sample preparation

Sediment cores were taken during R/V Sonne expedition SO292/2[26] in 2022 using a gravity corer equipped with a ~1400 kg weight stack. After retrieval and opening of the cores, the sediment was sampled using steel spatulas (thoroughly cleaned with ultrapure de-ionized water and methanol and stored in 50 mL Falcon™ tubes at −20 °C. For further details on the sampling protocol see Menapace et al.[26]. After arrival of the cores at MARUM – Center for Marine Environmental Sciences, University of Bremen, Germany, they were stored at 4 °C. All IPL and core lipid quantitative analyses and most of the compound-specific $\delta^{13}C$ analyses were conducted on frozen cores. As not enough frozen sample material was available to conduct lipid isotope analyses on all depths, additional sample material stored at 4 °C was used (specifically for depth 140–160 cm). Chromatograms from gas chromatography and $\delta^{13}C$ values for the archaeal and bacterial ether lipids in select samples extracted after 24 months of storage at 4 °C were identical to those obtained from the frozen cores. This indicated that isotopic signals of our target compounds remained stable during storage and were not altered by potential post-sampling microbial alteration at 4 °C. There are several factors that have likely kept any microbial activity in these cores at a bare minimum, these include removal of pore waters during onboard sampling, low TOC content of the serpentinite muds (<0.01 wt.%), and the strongly redox-dependent nature of the in-situ microbial community, which is unlikely to be reactivated under oxygenated storage conditions.

All samples were subjected to lyophilization (freeze-drying) for 24 h. Subsequently, the samples were pulverized in a mill, ensuring that the samples were well homogenized, enabling maximum surface area for further analyses. Between milling of the individual samples, pulverized combusted industrial washed sea sand (from VWR Chemicals) was treated as a procedural blank to check lab-borne contamination and to minimize cross-contamination between the samples. Prior to milling of each blank and sample, the milling cell was thoroughly cleaned with ultrapure de-ionized water, methanol, and dichloromethane (DCM). To limit cross-contamination between the individual blank–sample pairs, waste sand blanks were milled in between each blank-sample pair. All sample preparation was carried out in the Hinrichs Lab at MARUM.

Mineral characterization

To assess mineral assemblages in mud samples from our sediment cores, powdered samples were subjected to X-ray diffraction (XRD) analyses for a semi-quantitative assessment of the mineral composition within the mud samples. Measurements were carried out at the Crystallography & Geomaterials Research Group, Faculty of Geosciences, University of Bremen, Germany using an X-ray diffractometer equipped with a Cu-tube (k(alpha) 1.541 Å, 45 kV, 40 mA) and a fixed divergence slit (¼°2θ) all maintained at approximately 25 °C. Peak identification and semi-quantification were executed using the Philips software X'Pert HighscoreTM[117]. XRD measurements were carried out employing a standardized Philips/Panalytical backloading system, which ensured a nearly random distribution of sample particles during sample preparation. Measurements spanned from 3° to 65°2θ, with a calculated step size of 0.017°θ and a corresponding time per step of 100 s.

To further refine the XRD data and assess the presence of hydrated minerals such as brucite and iowaite, thermogravimetry analyses (TGA) were carried out on the mud samples from cores GeoB24917-1 and GeoB24930-1. Brucite can be detected and quantified at abundances as low as 0.3%, offering greater sensitivity compared to XRD analyses[118]. Analyses were carried out at the Woods Hole Oceanographic Institution, Woods Hole (MA), U.S.A., using a Thermal Analysis (TA) Instruments SDT Q600 simultaneous thermogravimetric analyzer. We used approximately 40-50 mg of finely ground (70 microns passing) samples, which were then weighed into alumina crucibles and subjected to heating from room temperature to 1105 °C at a rate of 10 °C min^{-1}, concurrently monitoring changes in mass and heat flow. Nitrogen (N_2) was utilized as the purge gas,

at a flow rate of 50 mL min^{-1} to avoid oxidation of the samples. To minimize errors in sample weighing during the heating process, empty crucibles were measured as blank values simultaneously with each sample.

Pore water chemistry

Pore water sampling was carried out on sediment core whole-round sections onboard R/V Sonne during expedition SO292/2[26]. The first meter of every core was sampled at a 10 cm resolution, deeper in the cores pore water samples were taken every 20 cm. We used rhizon samplers (5 cm length, 0.15 µm porous polymer) attached to syringes to extract pore water from cores by creating a vacuum (cf[119].). Small holes were drilled in the core liners to insert the rhizons into the sediments. The rhizons were soaked in distilled water before use. Samples for anion concentrations measurements were stored in 2 mL air-tight Eppendorf® vials at 4 °C until their post-cruise analyses.

Pore water chemistry was measured in the Sediment Geochemistry laboratory at MARUM. Pore water SO_4^{2-} concentrations were determined by ion chromatography (Metrohm 861 Advanced Compact IC, Metrohm A Supp 5 column, 0.8 mL min^{-1}, conductivity detection after chemical suppression) in samples diluted 1:40 with Milli-Q-grade H_2O. The detection limit for SO_4^{2-} was 0.5 µM, with a precision of <1%.

Carbon concentrations and stable isotope analyses

TOC and total carbon (TC) contents and stable carbon isotopes of TOC ($\delta^{13}C_{TOC}$) were determined in the Hinrichs Lab at MARUM using a continuous-flow Thermo Finnigan Flash EA 2000 elemental analyzer coupled to Delta V plus isotope ratio mass spectrometer (IRMS). Prior to analysis, samples were subjected to overnight treatment with 10% (w/v) hydrochloric acid (HCl) to eliminate carbonate mineralization[120]; upon complete decarbonation, samples were rinsed to neutral pH using ultrapure de-ionized water. The processed samples were freeze-dried, weighed (30–40 mg), and then encapsulated in tin capsules (5 × 8 mm) for introduction into the elemental analyzer. Replicate measurements were carried out for each sample with a strict five-point calibration using an internal lab standard. The carbon isotope values are reported in delta notation relative to Vienna-Pee Dee Belemnite (V-PDB) standard. Five-point calibration was achieved using an estuarine sediment with known TOC and $\delta^{13}C_{TOC}$ as lab internal (4.6 wt.% TOC with $\delta^{13}C_{TOC}$ of −24.1‰ vs V-PDD). The standard deviation of $\delta^{13}C_{TOC}$ measured for the internal standard is 0.11 with an accuracy of 0.98. The TOC detection limit on the EA is 20 µg of carbon per tin capsule, equivalent to 0.05 wt.% in a 40 mg sample.

Lipid extraction, preparation of lipid fractions, and ether cleavage

A modified[121] Bligh and Dyer (B&D)[122] extraction protocol was employed to isolate all the polar compounds from the sample. All lipid extractions and preparation of lipid fractions were carried out in the Hinrichs Lab at MARUM. Approximately, 18-35 g of homogenized and pulverized freeze-dried sample material was sonicated with an ultrasonic stick for 10 min in subsequent three step B&D mixtures [2x methanol:DCM:PO_4 buffer (2:1:0.8, v:v:v), 1x methanol:DCM:TCA buffer solution (2:1:0.8, v:v:v), 1x DCM:methanol (3:1, v:v) (~ 30 mL each)] in a polytetrafluoroethylene screw cap bottle. The B&D mixtures were made using phosphate (PO_4) buffer (8.7 g K_2HPO_4 L^{-1} ultrapure de-ionized water at pH 7.4) and TCA (trichloroacetic acid) buffer (50 g TCA L^{-1} ultrapure de-ionized water at pH 2). Upon centrifugation, the supernatant was pooled in a separatory funnel, to which equal amounts of DCM and ultrapure de-ionized water were added and allowed to separate into an organic and an aqueous phase. The organic phase was drawn into an Erlenmeyer flask, followed by three subsequent washings of the aqueous phase with DCM. The collected organic phase was finally washed thrice with ultrapure de-ionized water, collected in a TurboVap® vial, and evaporated under a gentle stream of N_2 and concentrated in 4 mL vials. The total lipid extracts (TLEs) were stored in 4 mL vials at −20°C until further analysis.

Before gas chromatography-mass spectrometry (GC-MS) analyses, TLE aliquots were base-hydrolyzed using 6% methanolic potassium hydroxide (KOH) at 80 °C for 3 h to separate neutral lipid fractions (alcohols) and fatty acid fractions (fatty acid salts) (Supplementary Methods 2.2, Supplementary Fig. 12a). Prior to injection into the GC-MS, alcohols were derivatized with N,O-bis(trimethylsilyl)trifluoroacetamide (BSTFA) in pyridine at 70 °C for 1 h (Supplementary Methods 2.2, Supplementary Fig. 12b), and fatty acids were methylated with 20% boron trifluoride (BF_3) in methanol at 70 °C for 1 h, forming fatty acid methyl esters (FAMEs) (Supplementary Methods 2.2, Supplementary Fig. 12c). High molecular weight ether lipids, including GDGTs, underwent ether cleavage through acid-catalyzed nucleophilic substitution using 1.0 M boron tribromide (BBr_3) in DCM under a steady N_2 stream at 60 °C for 2 h. The resulting bromoalkanes were subsequently reduced to hydrocarbons by reacting with 1 mL of Super-Hydride solution (1.0 M lithium triethylborohydride in tetrahydrofuran (THF) under a N_2 stream at 60 °C for 2 h (Supplementary Methods 2.2, Supplementary Fig. 12d).

High-performance Liquid Chromatography-Mass Spectrometry (HPLC-MS)

The samples, along with their respective sand blanks, were analyzed to identify microbial membrane lipids using HPLC-MS. Untreated TLE aliquots underwent screening for various archaeal and bacterial IPLs and core lipids through a full scan mode of a Dionex Ultimate 3000 UHPLC instrument coupled to a Bruker MaXis ultra-high resolution quadrupole time-of-flight mass spectrometer (UHR-QTOF-MS) at Hinrichs Lab at MARUM. Archaeal core lipids, archaeal tetraether IPLs, and bacterial core non-isoprenoid di- and tetraether lipids were detected and quantified using modified Reverse Phase-Electrospray Ionization-MS (RP-ESI-MS); whereas, bacterial IPLs and archaeal intact diether lipids were detected using Hydrophilic Interaction liquid Chromatography coupled with ESI-MS (HILIC-ESI-MS); the details of which are listed in Supplementary Table 5. The HILIC-ESI-MS method was more sensitive than RP-ESI-MS for detecting archaeal IPLs, however, only RP-ESI-MS method separates tetraether rings. The MS was set to positive ion mode with a mass-to-charge ratio (*m/z*) range of 500-2000.

The HPLC-MS data was analyzed with Data Analysis 4.4 (Bruker Daltonics, Bremen, Germany). MS2 fragments were created using data-dependent mode. Compounds were identified according to their exact masses in the MS1 as well as their retention times and fragmentation patterns when available. Bacterial origin DEG peaks were identified using their exact *m/z*, retention time, and diagnostic MS2 spectra (Supplementary Methods 2.3). Each spectrum was calibrated with a lock mass (*m/z* 922.0098), achieving a final mass accuracy below 1 ppm. For quantification, an external calibration (Supplementary Figs. 13, 14) was achieved with commercially available standards (PE-DAG C32:0, PG-DAG C32:0, PME-DAG C32:0, PDME-DAG C32:0, DGTS-DAG C32:0, PC-DEG C32:0, 1G-DAG C32:1, 1G-AR, 2G-AR, 1G-GDGT-0, C-GDGT-0, C-AR and C-DEG C32:0). For compounds lacking an available standard, slopes were assigned based on structural similarity to existing standards. A summary of slope assignments for the detected compound classes can be found in Supplementary Table 6. To account for potential lab-based contamination, the peak areas of compound of interest were corrected by subtracting the corresponding peak areas if observed in blanks. Quantification was carried out utilizing equations (3), (4) and (5) mentioned in Supplementary Methods 2.4. As a preventive measure, each sand blank's TLE was analyzed before its corresponding sample TLE to prevent potential cross-contamination. Additionally, regular analytical blanks, involving the injection of methanol only, were analyzed to identify any potential instrument-related contamination during measurements.

Gas Chromatography-Mass Spectrometry (GC-MS)

All GC-MS analyses were carried out in the Hinrichs Lab at MARUM. Compounds in the alcohol and ether-cleaved fractions were identified using an Agilent 7890 gas chromatograph fitted with a programmable temperature vaporizing (PTV) injector operated in splitless mode and equipped with a Varian CPSil-5 fused silica capillary column (60 m length, 0.32 mm inner diameter, and 0.25 µm film thickness), coupled to an Agilent 5975 C mass-selective detector. Due to sample limitations, only ether-cleaved fractions

and specific standards for compounds of interest were analyzed on GC-MS to verify retention times. The column temperature was initially set to 60 °C with a constant flow rate of 2.5 mL min^{-1}, then ramped at a rate of 10 °C min^{-1} to reach 100 °C, followed by a temperature gradient of 4 °C min^{-1} to 320 °C, where it was held constant for 20 min.

Gas Chromatography Isotope Ratio Mass Spectrometry

Stable carbon isotopic compositions of selected lipids were analyzed in the Hinrichs Lab at MARUM using a Thermo TraceGC gas chromatograph with a PTV injector, paired with an Agilent J&W DB-1 fused silica capillary column (60 m length, 0.32 mm inner diameter, and 0.25 µm film thickness) connected to a ThermoFinnigan Deltaplus XL isotope ratio mass spectrometer via a combustion interface set to 850 °C. A temperature program similar to that of the GC-MS analyses was employed. The samples were hand-injected due to low sample volume. Carbon isotope ratios were measured against an external CO_2 standard, regularly calibrated with a reference *n*-alkane standard mixture. Isotopic values were corrected by mass balance to account for carbon introduced by trimethylsilyl or methyl derivatives where applicable utilizing equation (6) stated in Supplementary Methods 2.5. The compound-specific carbon isotopic values are reported in the delta notation as $\delta^{13}C$ relative to the Vienna Pee Dee Belemnite (V-PDB) standard.

Thermodynamic calculations

Gibbs free energy yields (ΔGr) were calculated for various methanogenic and non-methanogenic microbial metabolic pathways using the equation:

$$\Delta_r G = \Delta_r G^0{}_{(T,p)} + RT\ln Q_r \quad (1)$$

Where $\Delta_r G^0{}_{(T,p)}$ denotes standard Gibbs free energy of the given reaction, R is the gas constant and T is the temperature in Kelvin. Q_r represents the activity product of the reaction r, which accounts for the chemical composition of the fluid, which is expressed as:

$$Q_r = \Pi a_i^{vi,r} \quad (2)$$

Where a_i is the activity of species i, which accounts for the effective concentration of species in a non-ideal system, and $v_{i,r}$ is the reaction stoichiometric coefficient of species i, representing the moles of species participating in the reaction r. Values for $\Delta_r G^0{}_{(T,p)}$ were calculated at an assumed in-situ temperature of 2 °C[123], calculated in-situ pressure of 300 bars based on hydrostatic pressure assuming a seawater density of 1013 g cm^{-3} using SUPCRT92[124] at an in-situ pH of 10. The activities for aqueous species in the assumed fluid composition are listed in Supplementary Table 7, which were computed using the REACT module of Geochemist's Workbench® using a 250-bar database assembled using SUPCRT92[124].

Reporting summary

Further information on research design is available in the Nature Portfolio Reporting Summary linked to this article.

Data availability

All data used in this study is available in supplementary files and/or is accessible at https://doi.org/10.5281/zenodo.16536583 and https://doi.org/10.5281/zenodo.16562890.

Received: 2 May 2025; Accepted: 1 August 2025;
Published online: 13 August 2025

References

1. Bar-On, Y. M., Phillips, R. & Milo, R. The biomass distribution on Earth. *Proc. Natl. Acad. Sci.* **115**, 6506–6511 (2018).
2. Orcutt, B. N., Sylvan, J. B., Knab, N. J. & Edwards, K. J. Microbial Ecology of the Dark Ocean above, at, and below the Seafloor. *Microbiol. Mol. Biol. Rev.* **75**, 361–422 (2011).
3. Früh-Green, G. L. et al. Diversity of magmatism, hydrothermal processes and microbial interactions at mid-ocean ridges. *Nat. Rev. Earth Environ.* **3**, 852–871 (2022).
4. Takai, K. Limits of life and the biosphere: Lessons from the detection of microorganisms in the deep sea and deep subsurface of the Earth. In *Origins and Evolution of Life: An Astrobiological Perspective* (eds Gargaud, M., López-Garcìa, P. & Martin, H.), Vol. 6, 469–486 (2011).
5. Bach, W. et al. Unraveling the sequence of serpentinization reactions: Petrography, mineral chemistry, and petrophysics of serpentinites from MAR 15°N (ODP Leg 209, Site 1274). *Geophys. Res. Lett.* **33**, L13306 (2006).
6. McCollom, T. M. & Bach, W. Thermodynamic constraints on hydrogen generation during serpentinization of ultramafic rocks. *Geochim. Cosmochim. Acta* **73**, 856–875 (2009).
7. McCollom, T. M. Laboratory simulations of abiotic hydrocarbon formation in Earth's deep subsurface. *Rev. Mineral. Geochem.* **75**, 467–494 (2013).
8. Schulte, M., Blake, D., Hoehler, T. & Mccollom, T. Serpentinization and Its Implications for Life on the Early Earth and Mars. *Astrobiology* **6**, 364–376 (2006).
9. McCollom, T. M. & Seewald, J. S. Serpentinites, hydrogen, and life. *Elements* **9**, 129–134 (2013).
10. Amend, J. P., McCollom, T. M., Hentscher, M. & Bach, W. Catabolic and anabolic energy for chemolithoautotrophs in deep-sea hydrothermal systems hosted in different rock types. *Geochim. Cosmochim. Acta* **75**, 5736–5748 (2011).
11. Fujioka, K. et al. Serpentines as a capsule of the deep subsurface biosphere: evidence from the Chamorro Seamount, Mariana forearc. *JAMSTECH J. Deep Sea Res* **20**, 1–16 (2002).
12. Kelley, D. S. et al. A Serpentinite-Hosted Ecosystem: The Lost City Hydrothermal Field. *Science* **307**, 1428–1434 (2006).
13. Schrenk, M. O., Brazelton, W. J. & Lang, S. Q. Serpentinization, carbon, and deep life. *Rev. Miner. Geochem.* **75**, 575–606 (2013).
14. Lang, S. Q. & Brazelton, W. J. Habitability of the marine serpentinite subsurface: A case study of the Lost City hydrothermal field. *Philos. Trans. Royal Soc. A: Math. Phys. Eng. Sci.* **378**, 20180429 (2020).
15. Fryer, P. Serpentinite mud volcanism: Observations, processes, and implications. *Ann. Rev. Mar. Sci.* **4**, 345–373 (2012).
16. Fryer, P. et al. Mariana serpentinite mud volcanism exhumes subducted seamount materials: Implications for the origin of life. *Philos. Trans. Royal Soc. A: Math. Phys. Eng. Sci.* **378**, 20180425 (2020).
17. Mottl, M. J., McCollom, T. M., Wheat, C. G. & Fryer, P. Chemistry of springs across the Mariana forearc: Carbon flux from the subducting plate triggered by the lawsonite-to-epidote transition? *Geochim. Cosmochim. Acta* **340**, 1–20 (2023).
18. Mottl, M. J., Komor, S. C., Fryer, P. & Moyer, C. L. Deep-slab fluids fuel extremophilic Archaea on a Mariana forearc serpentinite mud volcano: Ocean drilling program leg 195. *Geochem. Geophys. Geosyst.* **4**, 9009 (2003).
19. Wheat, C. G., Seewald, J. S. & Takai, K. Fluid transport and reaction processes within a serpentinite mud volcano: South Chamorro Seamount. *Geochim Cosmochim. Acta* **269**, 413–428 (2020).
20. Eickenbusch, P. et al. Origin of short-chain organic acids in serpentinite mud volcanoes of the Mariana convergent margin. *Front. Microbiol.* **10**, 1729 (2019).
21. Sissmann, O. et al. Abiogenic formation of H2, light hydrocarbons and other short-chain organic compounds within the serpentinite mud volcanoes of the Marianna Trench. *E3S Web of Conferences* **98**, 02011 (2019).
22. Curtis, A. C., Wheat, C. G., Fryer, P. & Moyer, C. L. Mariana Forearc Serpentinite Mud Volcanoes Harbor Novel Communities of Extremophilic Archaea. *Geomicrobiol. J.* **30**, 430–441 (2013).
23. Yamanaka, T. et al. Stable isotope evidence for a putative endosymbiont-based lithotrophic Bathymodiolus sp. mussel

community atop a serpentine seamont. *Geomicrobiol. J.* **20**, 185–197 (2003).
24. Mullis, M. M. et al. Microbial survival mechanisms within serpentinizing Mariana forearc sediments. *FEMS Microbiol Ecol* **99**, fiad003 (2023).
25. Kawagucci, S. et al. Cool, alkaline serpentinite formation fluid regime with scarce microbial habitability and possible abiotic synthesis beneath the South Chamorro Seamount. *Prog. Earth Planet. Sci.* **5**, 1–20 (2018).
26. Menapace, W. et al. Characterization and Monitoring of Serpentinite Mud Volcanoes' Fluid/Solid Emissions in the Mariana Forearc. *SONNE-Berichte SO292/2* 1-134; https://doi.org/10.48433/cr_so292_2 (2022).
27. Snow', J. E. & Dick, H. J. B. Pervasive Magnesium Loss by Marine Weathering of Peridotite. *Geochim. Cosmochim. Acta* **5**, 464 (1995).
28. Klein, F., Humphris, S. E. & Bach, W. Brucite formation and dissolution in oceanic serpentinite. *Geochem. Perspect. Lett.* **16**, 1–5 (2020).
29. Aoyama, S. et al. Recycled Archean sulfur in the mantle wedge of the Mariana Forearc and microbial sulfate reduction within an extremely alkaline serpentine seamount. *Earth Planet Sci. Lett* **491**, 109–120 (2018).
30. France, R. L. Carbon-13 enrichment in benthic compared to planktonic algae: foodweb implications. *Mar. Ecol. Prog. Ser.* **124**, 307–312 (1995).
31. Harvey', H. R., Fallon', R. D. & Patton', J. S. The effect of organic matter and oxygen on the degradation of bacterial membrane lipids in marine sediments. *Geochim. Cosmochim. Acta* **50**, 795–804 (1986).
32. Schouten, S., Hopmans, E. C. & Sinninghe Damsté, J. S. The organic geochemistry of glycerol dialkyl glycerol tetraether lipids: A review. *Org. Geochem.* **54**, 19–61 (2013).
33. Elling, F. J. et al. Chemotaxonomic characterisation of the thaumarchaeal lipidome. *Environ. Microbiol.* **19**, 2681–2700 (2017).
34. Schubotz, F., Wakeham, S. G., Lipp, J. S., Fredricks, H. F. & Hinrichs, K. U. Detection of microbial biomass by intact polar membrane lipid analysis in the water column and surface sediments of the Black Sea. *Environ. Microbiol.* **11**, 2720–2734 (2009).
35. Xie, S., Lipp, J. S., Wegener, G., Ferdelman, T. G. & Hinrichs, K. U. Turnover of microbial lipids in the deep biosphere and growth of benthic archaeal populations. *Proc. Natl. Acad. Sci.* **110**, 6010–6014 (2013).
36. Evans, T. W. et al. Size and composition of subseafloor microbial community in the Benguela upwelling area examined from intact membrane lipid and DNA analysis. *Org. Geochem* **111**, 86–100 (2017).
37. Taipale, S. J. et al. Inferring phytoplankton, terrestrial plant and bacteria bulk δ13 C values from compound specific analyses of lipids and fatty acids. *PLoS One* **10**, e0133974 (2015).
38. Lipp, J. S. & Hinrichs, K. U. Structural diversity and fate of intact polar lipids in marine sediments. *Geochim. Cosmochim. Acta* **73**, 6816–6833 (2009).
39. Bradley, A. S., Fredricks, H., Hinrichs, K. U. & Summons, R. E. Structural diversity of diether lipids in carbonate chimneys at the Lost City Hydrothermal Field. *Org. Geochem.* **40**, 1169–1178 (2009).
40. Lincoln, S. A., Bradley, A. S., Newman, S. A. & Summons, R. E. Archaeal and bacterial glycerol dialkyl glycerol tetraether lipids in chimneys of the Lost City Hydrothermal Field. *Org. Geochem.* **60**, 45–53 (2013).
41. Gibson, R. A. et al. Comparison of intact polar lipid with microbial community composition of vent deposits of the Rainbow and Lucky Strike hydrothermal fields. *Geobiology* **11**, 72–85 (2013).
42. Zwicker, J. et al. Evidence for archaeal methanogenesis within veins at the onshore serpentinite-hosted Chimaera seeps, Turkey. *Chem. Geol.* **483**, 567–580 (2018).
43. Newman, S. A. et al. Lipid Biomarker Record of the Serpentinite-Hosted Ecosystem of the Samail Ophiolite, Oman and Implications for the Search for Biosignatures on Mars. *Astrobiology* **20**, 830–845 (2020).
44. Rattray, J. E., Zetterlind, A., Smittenberg, R. H., Potiszil, C. & Neubeck, A. Complexity of the serpentinization lipidome. *Org. Geochem.* **174**, 104514 (2022).
45. Rempfert, K. R. et al. Subsurface biogeochemical cycling of nitrogen in the actively serpentinizing Samail Ophiolite, Oman. *Front. Microbiol.* **14**, 1139633 (2023).
46. Koga, Y. & Morii, H. Recent Advances in Structural Research on Ether Lipids from Archaea Including Comparative and Physiological Aspects. *Biosci. Biotechnol. Biochem* **69**, 2019–2034 (2005).
47. Hinrichs, K. U., Hayes, J. M., sylva, S. P., Brewer, P. & DeLong, E. F. Methane-consuming archaebacteria in marine sediments. *Nature* **398**, 802–805 (1999).
48. Hinrichs, K.-U. & Boetius, A. The anaerobic oxidation of methane: new insights in microbial ecology and biogeochemistry. In *Ocean Margin Systems* (eds Wefer, G. et al.), 457–477 (2002).
49. Aloisi, G. et al. CH_4-consuming microorganisms and the formation of carbonate crusts at cold seeps. *Earth Planet. Sci. Lett.* **203**, 195–203 (2002).
50. Blumenberg, M., Seifert, R., Reitner, J., Pape, T. & Michaelis, W. Membrane Lipid Patterns Typify Distinct Anaerobic Methanotrophic Consortia. *Proc. Natl. Acad. Sci. USA* **101**, 11111–11116 (2004).
51. Rossel, P. E. et al. Intact polar lipids of anaerobic methanotrophic archaea and associated bacteria. *Org. Geochem.* **39**, 992–999 (2008).
52. Pearson, A. & Ingalls, A. E. Assessing the use of archaeal lipids as marine environmental proxies. *Annu. Rev. Earth Planet. Sci.* **41**, 359–384 (2013).
53. Vinçon-Laugier, A., Grossi, V., Pacton, M., Escarguel, G. & Cravo-Laureau, C. The alkyl glycerol ether lipid composition of heterotrophic sulfate reducing bacteria strongly depends on growth substrate. *Org. Geochem.* **98**, 141–154 (2016).
54. Langworthy, T. A., Holzer, G., Zeikus, J. G. & Tornabene, T. G. Iso- and Anteiso-Branched Glycerol Diethers of the Thermophilic Anaerobe Thermodesulfotobacterium commune. *Syst. Appl. Microbiol.* **4**, 1–17 (1983).
55. Bradley, A. S., Hayes, J. M. & Summons, R. E. Extraordinary ^{13}C enrichment of diether lipids at the Lost City Hydrothermal Field indicates a carbon-limited ecosystem. *Geochim. Cosmochim. Acta* **73**, 102–118 (2009).
56. Weijers, J. W. H. et al. Membrane lipids of mesophilic anaerobic bacteria thriving in peats have typical archaeal traits. *Environ. Microbiol.* **8**, 648–657 (2006).
57. Kellermann, M. Y. et al. Autotrophy as a predominant mode of carbon fixation in anaerobic methane-oxidizing microbial communities. *Proc. Natl. Acad. Sci. USA*. **109**, 19321–19326 (2012).
58. Wheat, C. G. et al. Borehole observations of fluid flow from South Chamorro Seamount, an active serpentinite mud volcano in the Mariana forearc. *Earth Planet. Sci. Lett* **267**, 401–409 (2008).
59. Pancost, R. D. et al. Three series of non-isoprenoidal dialkyl glycerol diethers in cold-seep carbonate crusts. *Org. Geochem* **32**, 695–707 (2001).
60. Londry, K. L. & Des Marais, D. J. Stable carbon isotope fractionation by sulfate-reducing bacteria. *Appl Environ. Microbiol.* **69**, 2942–2949 (2003).
61. Londry, K. L., Jahnke, L. L. & Des Marais, D. J. Stable carbon isotope ratios of lipid biomarkers of sulfate-reducing bacteria. *Appl. Environ. Microbiol.* **70**, 745–751 (2004).
62. Haroon, M. F. et al. Anaerobic oxidation of methane coupled to nitrate reduction in a novel archaeal lineage. *Nature* **500**, 567–570 (2013).

63. Arshad, A. et al. A metagenomics-based metabolic model of nitrate-dependent anaerobic oxidation of methane by Methanoperedens-like archaea. *Front. Microbiol.* **6**, 1423 (2015).
64. Raghoebarsing, A. A. et al. A microbial consortium couples anaerobic methane oxidation to denitrification. *Nature* **440**, 918–921 (2006).
65. Knittel, K. & Boetius, A. Anaerobic oxidation of methane: Progress with an unknown process. *Ann. Rev. Microbiol.* **63**, 311–334 (2009).
66. Cui, M., Ma, A., Qi, H., Zhuang, X. & Zhuang, G. Anaerobic oxidation of methane: An 'active' microbial process. *MicrobiologyOpen* **4**, 1–11 (2015).
67. Yücel, M. et al. Nitrate and nitrite variability at the seafloor of an oxygen minimum zone revealed by a novel microfluidic in-situ chemical sensor. *PLoS One* **10**, e0132785 (2015).
68. Biddle, J. F. et al. Heterotrophic Archaea Dominate Sedimentary Subsurface Ecosystems off Peru. *Proc. Natl. Acad. Sci. USA*. **103**, 3846–3851 (2006).
69. Hoehler, T. M., Alperin, M. J., Albert, D. B. & Martens, C. S. Thermodynamic control on hydrogen concentrations in anoxic sediments. *Geochim Cosmochim. Acta* **62**, 1745–1756 (1998).
70. Proskurowski, G. et al. Abiogenic Hydrocarbon Production at Lost City Hydrothermal Field. *Science* **319**, 604–607 (2008).
71. Lang, S. Q. et al. Deeply-sourced formate fuels sulfate reducers but not methanogens at Lost City hydrothermal field. *Sci. Rep.* **8**, 755 (2018).
72. Coskun, Ö. K. et al. Quantifying the effects of hydrogen on carbon assimilation in a seafloor microbial community associated with ultramafic rocks. *ISME J* **16**, 257–271 (2022).
73. McDowall, J. S. et al. Bacterial formate hydrogenlyase complex. *Proc. Natl. Acad. Sci. USA* **111**, E3948–E3956 (2014).
74. Londry, K. L., Dawson, K. G., Grover, H. D., Summons, R. E. & Bradley, A. S. Stable carbon isotope fractionation between substrates and products of Methanosarcina barkeri. *Org. Geochem* **39**, 608–621 (2008).
75. House, C. H., Schopf, J. W. & Stetter, K. O. Carbon Isotopic Fractionation by Archaeans and Other Thermophilic Prokaryotes. *Org. Geochem.* **34**, 345–356 (2003).
76. Thauer, R. K. & Morris, J. G. Metabolism of chemotrophic anaerobes: old views and new aspects. *Symposia of the Society for General Microbiology (Cambridge)* (1984).
77. Mausz, M. A. & Chen, Y. Microbiology and ecology of methylated amine metabolism in marine ecosystems. *Curr. Issues Mol. Biol.* **33**, 133–148 (2019).
78. King, G. M. Metabolism of Trimethylamine, Choline, and Glycine Betaine by Sulfate-Reducing and Methanogenic Bacteria in Marine Sediments. *Appl. Environ. Microb.* **48**, 719–725 (1984).
79. Kallistova, A. Y., Merkel, A. Y., Tarnovetskii, I. Y. & Pimenov, N. V. Methane formation and oxidation by prokaryotes. *Microbiology* **86**, 671–691 (2017).
80. Fones, E. M. et al. Diversification of methanogens into hyperalkaline serpentinizing environments through adaptations to minimize oxidant limitation. *ISME J* **15**, 1121–1135 (2021).
81. Wood, G. E., Haydock, A. K. & Leigh, J. A. Function and regulation of the formate dehydrogenase genes of the methanogenic archaeon Methanococcus maripaludis. *J. Bacteriol.* **185**, 2548–2554 (2003).
82. Kaster, A. K. et al. More than 200 genes required for methane formation from H_2 and CO_2 and energy conservation are present in methanothermobacter marburgensis and methanothermobacter thermautotrophicus. *Archaea* **2011**, 973848 (2011).
83. Reeburgh, W. S. Oceanic methane biogeochemistry. *Chem. Rev.* **107**, 486–513 (2007).
84. Twing, K. I. et al. Serpentinization-influenced groundwater harbors extremely low diversity microbial communities adapted to high pH. *Front. Microbiol.* **8**, 308 (2017).
85. Alt, J. C. & Teagle, D. A. H. The Uptake of Carbon during Alteration of Ocean Crust. *Geochim. Cosmochim. Acta* **63**, 1527–1535 (1999).
86. Clift, P. D. A revised budget for Cenozoic sedimentary carbon subduction. *Rev. Geophys.* **55**, 97–125 (2017).
87. Albers, E. et al. Fluid-rock interactions in the shallow Mariana forearc: Carbon cycling and redox conditions. *Solid Earth* **10**, 907–930 (2019).
88. Conrad, R. Contribution of hydrogen to methane production and control of hydrogen concentrations in methanogenic soils and sediments. *FEMS Microbiol. Ecol.* **28**, 193–202 (1999).
89. Valentine, D. L. Adaptations to energy stress dictate the ecology and evolution of the Archaea. *Nat. Rev. Microbiol.* **5**, 316–323 (2007).
90. Siliakus, M. F., van der Oost, J. & Kengen, S. W. M. Adaptations of archaeal and bacterial membranes to variations in temperature, pH and pressure. *Extremophiles* **21**, 651–670 (2017).
91. Schubotz, F., Sephton, M. A. & & Derenne Sylvie. Biomarkers in Extreme Environments on Earth and the Search for Extraterrestrial Life in Our Solar System. *Elements* **18**, 100–106 (2022).
92. Schubotz, F. et al. Stable isotope labeling confirms mixotrophic nature of streamer biofilm communities at alkaline hot springs. *Front. Microbiol.* **6**, 42 (2015).
93. Li, J. et al. Rcycling and metabolic flexibility dictate life in the lower oceanic crust. *Nature* **579**, 250–255 (2020).
94. Boyer, G. M., Schubotz, F., Summons, R. E., Woods, J. & Shock, E. L. Carbon Oxidation State in Microbial Polar Lipids Suggests Adaptation to Hot Spring Temperature and Redox Gradients. *Front. Microbiol.* **11**, 229 (2020).
95. Bosak, T. et al. System-wide adaptations of Desulfovibrio alaskensis G20 to phosphate-limited conditions. *PLoS One* **11**, e0168719 (2016).
96. Templeton, A. S. et al. Accessing the Subsurface Biosphere Within Rocks Undergoing Active Low-Temperature Serpentinization in the Samail Ophiolite (Oman Drilling Project). *J. Geophys. Res. Biogeosci* **126**, e2021JG006315 (2021).
97. Templeton, A. S. & Ellison, E. T. Formation and loss of metastable brucite: Does Fe(II)-bearing brucite support microbial activity in serpentinizing ecosystems? *Philos. Trans. R. Soc. A* **378**, 20180423 (2020).
98. Shimada, H., Nemoto, N., Shida, Y., Oshima, T. & Yamagishi, A. Effects of pH and temperature on the composition of polar lipids in Thermoplasma acidophilum HO-62. *J. Bacteriol.* **190**, 5404–5411 (2008).
99. Kanduč, M. et al. Tight cohesion between glycolipid membranes results from balanced water-headgroup interactions. *Nat. Commun.* **8**, 14899 (2017).
100. Yoshinaga, M. Y. et al. Methanothermobacter thermautotrophicus modulates its membrane lipids in response to hydrogen and nutrient availability. *Front. Microbiol.* **6**, 5 (2015).
101. Kellermann, M. Y., Yoshinaga, M. Y., Wegener, G., Krukenberg, V. & Hinrichs, K. U. Tracing the production and fate of individual archaeal intact polar lipids using stable isotope probing. *Org. Geochem.* **95**, 13–20 (2016).
102. Macalady, J. L. et al. Tetraether-linked membrane monolayers in Ferroplasma spp: A key to survival in acid. *Extremophiles* **8**, 411–419 (2004).
103. Boyd, E. S. et al. Temperature and pH controls on glycerol dibiphytanyl glycerol tetraether lipid composition in the hyperthermophilic crenarchaeon Acidilobus sulfurireducens. *Extremophiles* **15**, 59–65 (2011).
104. Lloyd, K. G., Lapham, L. & Teske, A. An anaerobic methane-oxidizing community of ANME-1b archaea in hypersaline gulf of Mexico sediments. *Appl. Environ. Microbiol.* **72**, 7218–7230 (2006).
105. Zhou, A. et al. Energy flux controls tetraether lipid cyclization in Sulfolobus acidocaldarius. *Environ. Microbiol.* **22**, 343–353 (2020).

106. Pearson, A. et al. Factors controlling the distribution of archaeal tetraethers in terrestrial hot springs. *Appl Environ. Microbiol.* **74**, 3523–3532 (2008).
107. Bale, N. J. et al. New insights into the polar lipid composition of extremely halo(alkali)philic euryarchaea from hypersaline lakes. *Front. Microbiol.* **10**, 377 (2019).
108. Nichols, D. S. et al. Cold adaptation in the Antarctic archaeon Methanococcoides burtonii involves membrane lipid unsaturation. *J. Bacteriol.* **186**, 8508–8515 (2004).
109. Dawson, K. S., Freeman, K. H. & Macalady, J. L. Molecular characterization of core lipids from halophilic archaea grown under different salinity conditions. *Org. Geochem.* **48**, 1–8 (2012).
110. Weijers, J. W. H., Schefuß, E., Kim, J. H., Sinninghe Damsté, J. S. & Schouten, S. Constraints on the sources of branched tetraether membrane lipids in distal marine sediments. *Org. Geochem.* **72**, 14–22 (2014).
111. Pan, A. et al. A diagnostic GDGT signature for the impact of hydrothermal activity on surface deposits at the Southwest Indian Ridge. *Org. Geochem.* **99**, 90–101 (2016).
112. Liu, X. L., Zhu, C., Wakeham, S. G. & Hinrichs, K. U. In situ production of branched glycerol dialkyl glycerol tetraethers in anoxic marine water columns. *Mar. Chem.* **166**, 1–8 (2014).
113. Weijers, J. W. H., Schouten, S., van den Donker, J. C., Hopmans, E. C. & Sinninghe Damsté, J. S. Environmental controls on bacterial tetraether membrane lipid distribution in soils. *Geochim Cosmochim. Acta* **71**, 703–713 (2007).
114. Peterse, F., Nicol, G. W., Schouten, S. & Sinninghe Damsté, J. S. Influence of soil pH on the abundance and distribution of core and intact polar lipid-derived branched GDGTs in soil. *Org. Geochem.* **41**, 1171–1175 (2010).
115. Halamka, T. A. et al. Oxygen limitation can trigger the production of branched GDGTs in culture. *Geochem. Perspect. Lett.* **19**, 36–39 (2021).
116. Plümper, O. et al. Subduction zone forearc serpentinites as incubators for deep microbial life. *Proc. Natl. Acad. Sci.* **114**, 4324–4329 (2017).
117. Degen, T., Sadki, M., Bron, E., König, U. & Nénert, G. The high score suite. *Powder Diffr.* **29**, S13–S18 (2014).
118. Turvey, C. C., Wynands, E. R. & Dipple, G. M. A new method for rapid brucite quantification using thermogravimetric analysis. *Thermochim. Acta* **718**, 179366 (2022).
119. Dickens, G. R., Koelling, M., Smith, D. C. & Schnieders, L. Rhizon sampling of pore waters on scientific drilling expeditions: an example from the IODP Expedition 302, Arctic Coring Expedition (ACEX). *Sci. Drill.* **4**, 22–25 (2007).
120. Brodie, C. R. et al. Evidence for bias in C and N concentrations and $\delta^{13}C$ composition of terrestrial and aquatic organic materials due to pre-analysis acid preparation methods. *Chem. Geol.* **282**, 67–83 (2011).
121. Sturt, H. F., Summons, R. E., Smith, K., Elvert, M. & Hinrichs, K. U. Intact polar membrane lipids in prokaryotes and sediments deciphered by high-performance liquid chromatography/ electrospray ionization multistage mass spectrometry - New biomarkers for biogeochemistry and microbial ecology. *Rapid Commun. Mass Spectrom.* **18**, 617–628 (2004).
122. Bligh, E. G. & Dyer, W. J. A rapid method of total lipid extraction and purification. *Can. J. Biochem. Physiol.* **37**, 911–917 (1959).
123. Mottl, M. J., Wheat, C. G., Fryer, P., Gharib, J. & Martin, J. B. Chemistry of springs across the Mariana forearc shows progressive devolatilization of the subducting plate. *Geochim. Cosmochim. Acta* **68**, 4915–4933 (2004).
124. Johnson, J. W., Oelkers, E. H. & Helgeson, H. C. Supcrt92: a software package for calculating the standard molal thermodynamic properties of minerals, gases, aqueous species, and reactions from 1 to 5000 bar and 0 to 1000 °C. *Comput. Geosci.* **18**, 899–947 (1992).
125. GEBCO Bathymetric Compilation Group 2024. The GEBCO_2024 Grid - a continuous terrain model of the global oceans and land. 2024. *NERC EDS British Oceanographic Data Centre NOC*. https://doi.org/10.5285/1c44ce99-0a0d-5f4f-e063-7086abc0ea0f (2024).

Acknowledgements

We extend our gratitude to the captain, crew, and science party of R/V *Sonne* during expedition SO292/2 for their support. Special thanks go to Jenny Altun for assistance with carbon isotope analyses, Julius Lipp, Julia Cordes, and Lukas Dirksen for their assistance with HPLC-MS analyses, and Matthias Zabel for conducting pore water chemistry analyses. We thank Marcus Elvert and Victoria Kürzinger for data interpretation feedback and Anne-Sophie Plessgott for help with lab work. We thank the United States Department of State, Bureau of Oceans and International Environmental and Scientific Affairs, and the Mariana Trench Marine National Monument for granting the sampling permit (Permit No. U2022-003). We thank MARUM GeoB Core Collection for providing access to the archived cores for re-sampling. This research was funded by the German Research Foundation (Deutsche Forschungsgemeinschaft; DFG), project no. 453470886 to E.A. and W.B., and was supported by the Cluster of Excellence 'The Ocean Floor – Earth's Uncharted Interface', project no. 390741603. P.K. acknowledges MARUM Research Academy (formerly known as GLOMAR Graduate School) for providing training and travel support. W.M. and E.A. acknowledge funding from the Federal Ministry of Education and Research (Bundesministerium für Bildung und Forschung; BMBF) for the SO292/2 expedition (grant #03G0292TA) and W.M. from the Austrian Science Fund (Österreichischer Wissenschaftsfonds; FWF) for his own position during the same expedition (grant #M 3146-417 N).

Author contributions

The sample recovery was carried out by joint efforts of P.K., W.M., E.A., and W.B. Sample processing and biomarker analyses were conducted by P.K. at MARUM – Center for Marine Environmental Sciences under the guidance of F.S., E. A and W.B. Analyses at Woods Hole Oceanographic Institution were also carried out by P.K., with access and oversight provided by F.K. Mineral characterization via XRD was conducted by C.V. Manuscript writing was led by P.K., while all co-authors (C.V., E.A., F.K., F.S., W.B., W.M.) provided essential feedback and contributions that shaped the research, analysis, and final manuscript.

Funding

Open Access funding enabled and organized by Projekt DEAL.

Competing interests

The authors declare no competing interests.

Additional information

Supplementary information The online version contains supplementary material available at https://doi.org/10.1038/s43247-025-02667-6.

Correspondence and requests for materials should be addressed to Palash Kumawat.

Peer review information *Communications Earth & Environment* thanks the anonymous reviewers for their contribution to the peer review of this work. Primary Handling Editors: D'Arcy Meyer-Dombard and Alice Drinkwater. A peer review file is available